Quart. J. R. Met. Soc. (1973), **99**, pp. 2-34

551.509.313

A numerical experiment using a general circulation model of the atmosphere

By A. GILCHRIST, G. A. CORBY and R. L. NEWSON
Meteorological Office, Bracknell

(Manuscript received 17 February 1972; in revised form 14 August 1972)

SUMMARY

The general circulation model whose formulation is described in Corby *et al.* (1972) was integrated for 60 days from real data with January radiation and sea surface temperatures. The deficiencies of the model as a representation of the atmosphere were revealed by the extent and rate of the systematic changes as an equilibrium state was approached. For the first ten days, the model lost eddy kinetic energy, then gradually recovered and from about day 30 its tropospheric simulations both synoptically and in its time-mean cross-sections at various longitudes, had many realistic features; it failed, however, to maintain a substantial Siberian winter anticyclone. A major weakness, resulting from the use of a single level to represent the 0-200 mb layer, was the progressive deterioration of the model stratosphere.

1. INTRODUCTION

The formulation of a general circulation model has been described by Corby, Gilchrist and Newson (1972). The performance of the model has been assessed by examining the results of an extended time-integration started from real atmospheric conditions with specified time-invariant sea surface temperatures and solar parameters. The more usual procedure with a general circulation model is to start with an isothermal motionless atmosphere (Mintz 1965; Smagorinsky, Manabe and Holloway 1965; Kasahara and Washington 1971), and allow the motions to be created entirely during the integration. However, the use of an actual atmospheric situation, though it raises questions concerning the influence of the initial conditions on the final model state, has certain merits. As the time integration proceeds, there are systematic changes in the model variables, on a variety of time and space scales, as it rejects or modifies real atmospheric features and approaches its own inherent equilibrium state (or, possibly, one of its equilibrium states). The changes, since they arise directly from the differences between the atmosphere's and the model's general circulations, reveal the deficiencies of the model as a representation of the atmosphere in a comparatively short period of integration.

Certain of the long term changes to be expected can be inferred from the known deficiencies of general circulation models. In particular, since all models, apparently, exhibit the characteristic of having a stronger mean zonal motion than the atmosphere associated with a given eddy kinetic energy, it is to be expected that, for a time, the eddy energy will fall and the zonal energy rise; and that later, the eddy energy will increase to reach eventually the values required by the model's general circulation. Data concerning the extent of the fall in eddy energy, on the time scale of the changes, and on systematic differences between different parts of the spectrum, are of interest; particularly, they are of concern in any consideration of the possibility of using fairly simple general circulation models to provide indications about possible evolutions of the real atmosphere over extended periods of time.

As regards the effect of the initial state on the subsequent course of the integration, it is clear that any feature which survives to affect the motion after an extended period (~ 50 days) must be particularly stable. If we consider the total climatology of a model for a particular season to consist of all the states it could achieve at that season in an endless integration with a varying solar input, then it seems reasonable that the states achieved after 50 days or so in this experiment would form a significant part of that total climatology. Indeed, there seems to be no valid reason for assuming that an integration from rest would be more significant from this point of view.

In carrying out this experiment, therefore, we had several objectives.

Firstly, we wished to assess the effectiveness or correctness of the individual elements which entered into the formulation of the general circulation model. In large measure, this emerges from a consideration of the model's state after integrating for a substantial period, and is discussed in Section 5. However, the effect of the pseudo-viscosity term cannot easily be appreciated in this way. In view of its significance as a mechanism which might damp baroclinic instability unduly, this term may have an important bearing on some of our results, and, since a similar formulation has not previously been used in general circulation studies, it seemed desirable to consider its effects in some detail. This is done appropriately in Section 4, where the changes in energy during the integration are described; particularly, we illustrate the discrimination achieved with respect to wavelength.

Secondly, it was our intention to continue the integration either until an equilibrium state was achieved or as long as seemed necessary to provide an adequate description of the model's climatology. In the event, it was decided to terminate the integration at 60 days, when the lower levels of the model appeared to have reached a quasi-steady state but systematic changes were still going on at the highest level ($\sim$ 100 mb).

At this level, the zonal flow was by this time much stronger than in the atmosphere, and the temperatures were systematically cold at all latitudes. It was, of course, realized when formulating the model, that only the crudest simulation of the stratosphere could be hoped for with a vertical structure that included only one stratospheric level; but, at the time, the view was taken that the structure adopted was preferable to the obvious alternative (bearing in mind the acceptable number of levels in the vertical imposed by computing limitations), which was to eliminate the stratosphere by imposing an upper boundary condition at about the level of the tropopause. There seemed little point in extending the integration in order to reach an equilibrium state at a level where the simulation was already notably unrealistic, and, in any case, there must be doubts about the wisdom of continuing for an even longer period with the solar input fixed near its seasonal minimum (viz. January mean values). Apart therefore from reservations associated primarily with the highest level, for which a climatology was not established, we have considered the period 50-60 days to constitute a representative sample of the model's climatology and have studied its characteristics at this time in some detail. A period of ten days is perhaps rather short from some points of view; over as short a period there may be significant imbalances among quantities which must balance in the longer term, and particular synoptic events may be given undue significance. However, it is clear from an examination of the results that the model's range of behaviour is more restricted than the atmosphere's, and therefore, that in comparison with the latter, the difference between a ten day and a longer term mean is likely to be much less. This is a matter which so far has not received the attention it deserves in the literature, but it is, in all probability, a general feature of numerical models. Our judgement is that a ten day period is long enough to provide a reliable characterization of the model state near the end of the experiment, while the systematic changes between the beginning and end are acceptably small. The description of the model's variables for days 51-60 is in Section 5.

However, to supplement a description of the climatology derived in this way, and to gain further insight into the behaviour of the model, five-day mean cross-sections have been constructed for particular longitudes. For this purpose, it is neither necessary nor desirable to confine one's attention to days 51-60, since individual daily charts demonstrate that a reasonable simulation of many atmospheric phenomena had been achieved at a much earlier stage of the experiment (e.g. Gilchrist 1971). Moreover, it is not only average values that are of interest; the variability and stability of the model's flow patterns are as important, and information on these aspects is essential for a proper consideration of what experiments it is appropriate to attempt with general circulation models. In time, therefore, the cross-sections range over the second half of the integration. They enable us also to make an estimate of how realistically the model is able to reproduce the atmosphere's observed variations around lines of latitude. With this in mind, the longitudes chosen are

some for which mean data have been published. Comparisons with real data are bound, however, at this stage to be rather qualitative – whether, for instance the model produces two distinct jet-streams where two are usually observed in the atmosphere – since good quantitive agreement, even with comparable averaging periods, is hardly to be expected, and must be less good than corresponding comparisons of zonal averages. The variation of winds and temperatures is discussed in Section 3.

Thirdly, we were concerned to observe and try to understand the changes in the model with time, as a result of which there was a gradual approach to a quasi-steady state. Again, this is an important consideration for many experiments which might be attempted with general circulation models. Also, it should be noted that it may be of relevance even for forecasting models, since fairly large systematic changes can take place in a day or two, and a recognition of their nature could be of help in improving the forecast results. What one would like to achieve is a separation of the changes into those that are inevitable with a given grid separation, those that result from deficiencies of the finite difference approximation formulae, and those that are a result of shortcomings in the parameterization of physical effects, the objective being to eliminate the latter two categories. The separation cannot in general be made, and we have concentrated largely upon documenting the changes observed in this model, in the belief that changes in other models would be similar in nature, though varying in magnitude according to the grid size and the realism of the simulation of physical effects. These matters are considered mainly in Section 4.

2. Initial data

The atmospheric situation chosen as the starting conditions for the experiment were for 00 Z on 29 December 1965. The radiation constants were made appropriate to the mean January values, and were held constant throughout the integration. The sea surface temperature (Fig. 1) was also held constant with time. A smoothed version of the Earth's topography (Fig. 2) was assumed.

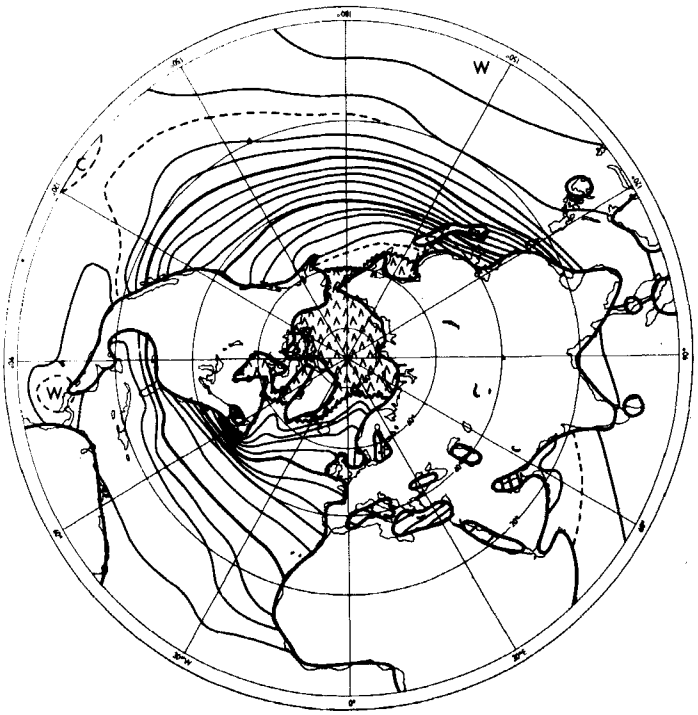

Figure 1. Sea surface isotherms, compiled from various published mean January maps, assumed by the model. The interval is 2°K with dashed lines to indicate additional intermediate values. The 10°C and 20°C isotherms are thickened. Λ indicates sea-ice.

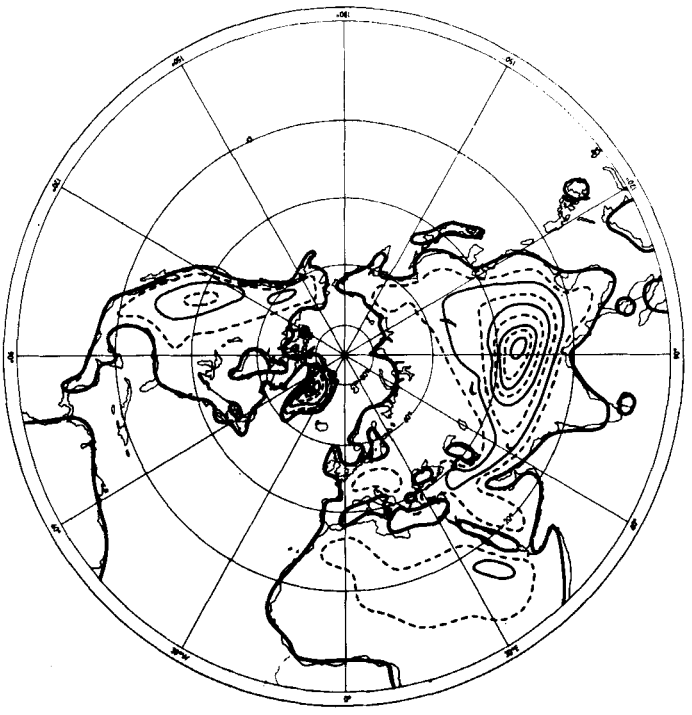

Figure 2. Topographic contours assumed by the model. The interval is 1,000 m, with dashed line to indicate intermediate 500 m values. The model coast-line is thickened.

The procedures adopted for determining winds and temperatures at the initial time are, perhaps, not crucial to the main objectives of the experiment, but they influence the behaviour of the model near the start of the integration and, therefore, a very brief description of them is given here.

Values of sea-level pressure and contour heights at standard levels (1,000, 850, 700, 500, 300 and 100mb) were taken from hemispheric charts, care being taken to avoid implied vertical static instabilities. Temperature at intermediate pressure levels $p = [p(\text{upper}).\ p(\text{lower})]^{\frac{1}{2}}$ were derived from the thickness equation

$$\Delta\phi = RT \log [p(\text{lower})/p(\text{upper})]\ ^{\dagger}$$

Over land, the surface pressure p_* and surface temperature T_* were derived from expressions (in which $\overline{T}$ was taken as the average of the upper and lower temperatures) for the thickness of the two parts of the pressure layer intersected by the Earth's surface. Then, by assuming a constant lapse between pressure levels for which the temperature was defined, temperatures on sigma surfaces were deduced. Moisture values for the grid points were taken from charts of relative humidity, with interpolation as necessary to find values on sigma surfaces. The humidity at the upper two levels was assumed zero initially.

In sigma co-ordinates, it is desirable to use initial horizontal winds for which the mass divergence $\nabla \cdot p_* \mathbf{V}$ (rather than, as is more usual, the divergence $\nabla \cdot \mathbf{V}$) is zero; particularly, this is necessary to avoid large surface pressure changes (a source of unwanted gravity waves) in the vicinity of mountains when the integration starts. Winds satisfying this property can be derived from a 'mass' stream function ψ where

$$p_* \mathbf{V} = \mathbf{k} \times \left(\frac{1}{\bar{f}}\right) \nabla \psi \quad . \quad . \quad . \quad . \quad (1)$$

$\bar{f}$ being a convenient scaling constant. ψ is to be found by solving a suitable balance equa-

† Where undefined, the symbols in this paper are the same as those used in Corby *et al.* (1972).

tion, which in this experiment was a form of the linearized balance equation on the sphere,

viz.
$$\left(\frac{f'}{\cos^2\theta}\right)\delta_\lambda\,\delta_\lambda\,\psi + \left(\frac{1}{\cos\theta}\right)\delta_\theta f' \cos\theta\,\delta_\theta\,\psi = \bar{f}\,F(\theta,\lambda) \quad . \quad . \quad (2)$$

where $f' = (f + u_G \tan\theta/a)$, u_G being the mean zonal geostrophic wind and

$$F(\theta,\lambda) = \left(\frac{1}{\cos^2\theta}\right)\delta_\lambda\,\overline{p_*}^{\lambda}\{\delta_\lambda\phi + R\overline{T}^{\lambda}\,\delta_\lambda \log p_*\} + \left(\frac{1}{\cos\theta}\right)\delta_\theta\,\overline{p_*}^{\theta}\cos\theta\{\delta_\theta\phi + R\overline{T}^{\theta}\,\delta_\theta \log p_*\} \quad . \quad . \quad (3)$$

In deriving the precise form of this equation, account has been taken of the finite difference expressions in the model equations. Because of the polar singularity, care has to be taken in solving Eq. (2) and we proceed as follows. Integrate Eq. (2) around lines of latitude to obtain

$$\delta_\theta f' \cos\theta\,\delta_\theta[\psi] = \bar{f}\,\delta_\theta[\overline{p_*}^{\theta}\cos\theta\{\delta_\theta\phi + R\overline{T}^{\theta}\,\delta_\theta \log p_*\}] \quad . \quad . \quad (4)$$

where [ ] denotes a zonal mean value.

Hence we solve

$$f'\,\delta_\theta[\psi] = \bar{f}\,[\overline{p_*}^{\theta}\{\delta_\theta\phi + R\overline{T}^{\theta}\,\delta_\theta \log p_*\}] \quad . \quad . \quad . \quad (5)$$

by quadrature for $[\psi]$, assuming an arbitrary value of $[\psi]$ at $1\frac{1}{2}$°N.

Starting from the initial axisymmetric guess $\psi = [\psi]$ for the appropriate line of latitude, the solution of Eq. (2) can be completed by an over-relaxation technique, the iterative scheme being designed so that $[\psi]$ values are not altered in the process. Values of u and v on sigma surfaces are deduced from

$$p_* u = -\left(\frac{1}{\bar{f}a}\right)\delta_\theta\,\overline{\psi}^{\theta}; \qquad p_* v = \left(\frac{1}{\bar{f}\,a\cos\theta}\right)\delta_\lambda\,\overline{\psi}^{\lambda} \quad . \quad . \quad (6)$$

The mass divergences (as calculated by the model's finite differences) resulting from this procedure are not precisely zero, but are acceptably small.

Because the non-linear terms have been neglected in deriving the winds, gravity waves occur in the early part of the integration, and lead to oscillations in the central pressures of synoptic systems during the first few hours. However, a condition of balance with respect to synoptic scale systems is achieved after a day or so. On the other hand, a large-scale axisymmetric gravity wave of initial amplitude about 1 mb in the surface pressure and corresponding in form and period to the expected P_2° external gravity wave (Longuet-Higgins 1968) was observed for a considerable part of the integration and its presence is evident in some of the energy and energy transformation statistics.

3. Wind and temperature variations

(a) *Zonal means*

There are some fairly rapid changes in the model's winds and temperatures at the beginning of the integration (see e.g. Fig. 5(a) to (e)). The maximum wind speed values decrease substantially within a day or two, due, presumably, to the viscosity term and to the dispersive effects of the finite differences. It can be conjectured that this is at least partly responsible for the failure to maintain sufficiently intense synoptic developments and the consequent fairly rapid fall in eddy kinetic energy during the first few days. (It is notable that later, with eddy energies restored and the mean zonal motion considerably stronger, the maximum wind speed values are more or less the same as at the beginning of the experiment.) To some extent, this degradation is already present in Fig. 3(a), which depicts the mean zonal winds and temperatures for days 1-5. From the point of view of the general circulation experiment, these mean data, in effect the model state after some initial rapid changes and with short period fluctuations removed, are representative of the zonal mean initial data presented to the model. They differ quite significantly from the January mean atmospheric conditions. In comparison with January mean zonal winds (Heastie and

Stephenson 1960), the wind maximum is less and further north (25·7 m s^{-1} at 40·5°N against 32 m s^{-1} at 32°N on the 300 mb surface); also the tropical easterlies are less extensive being indeed absent at 500 mb, and 300 mb. In comparison with January zonal mean temperatures (Crutcher 1971) the tropospheric temperatures are generally lower by 2-3°K, except (i) at 300 mb north of 40°N, where they are substantially higher (~5°K), (ii) at low levels in the Tropics and (iii) at 100 mb, where a relatively warm region (~215°K) at about 50°N is absent; this is caused by the initialization procedure which gives reasonable geopotential heights, but, being unable to recognize the presence of the tropopause, cannot at the same time give realistic temperatures for the top level.

For a period of about ten days, the zonal mean maximum wind weakened but this tendency was then reversed and throughout the remainder of the integration the maximum increased and moved to progressively lower latitudes. The 5-day mean cross-section for days 56-60 (Fig. 3(b)) shows an intense jet-stream structure, with a concentrated baroclinic zone in latitudes 20°-50°N. The wind maximum is now rather stronger than the January mean, but the latitude at which it occurs is about right. An obvious discrepancy between the model and the mean atmospheric cross-section is that the stronger wind shears are on the northern side of the jet-stream; while to the south weaker shear allows the westerlies to extend to the Equator at all but the lowest level. At 100 mb the winds are much too strong.

Fig. 3(c) shows the change in temperature between the two foregoing cross-sections. Almost everywhere there has been cooling, often substantial in amount. At the lowest level, the region of greatest cooling is at latitudes where there are large land masses, over which the surface temperatures are too low; thus at days 56-60 temperatures near 60°N over Asia are mostly around or a little below 230°K from 50°E to 140°E, a much more extensive area of low temperature than is actually found. The reasons for this are rather complex, being partly attributable locally to terms in the equation for T_*, but it may be just as important that the model flow is too zonal. (It has already been noted that generally models demand an over intense zonal flow to achieve dynamical equilibrium.) At 100 mb, there has been substantial cooling at all latitudes so that the model temperatures depart markedly from those of the atmosphere. To offset the fairly slow, but in the long term substantial, net radiational cooling at this level and so establish an equilibrium temperature distribution, it is necessary, in the absence of convective heating from below, for heat to be transported there from other levels by explicit vertical eddy or mean meridional motions. It is clear that for this to be adequately simulated, more stratospheric levels are required. It will also be noted that, since there is a monotonic decrease in temperature from Pole to Equator, the horizontal eddy transports and the eddy viscosity term are likely to cool the polar regions.

The pattern found by subtracting the January mean temperatures from those for days 56-60 is significantly different from that shown in Fig. 3(c). It has a large area of negative values in middle and high latitudes of the troposphere, with maximum −7° to −8°K at 500 mb at 50 N, and negative values everywhere in the stratosphere with maximum in excess of 20°K at the same latitude.

(*b*) *Longitudinal variation*

To illustrate the longitudinal variation of wind and temperature, we have chosen to show 5-day mean cross-sections at longitudes for which data have been published. Our main comparison is with Heastie and Stephenson (1960); our longitudes are coincident with theirs apart from 80°W, which we have preferred to 75°W. The relevant corresponding cross-section figure number in their publication is given for each section. The actual cross-sections are for periods throughout the integration; they have been chosen either because they are typical or because they illustrate some particular feature.

(i) 40°E (H & S Fig. 102). The atmospheric mean has two jet-streams – a rather intense subtropical maximum at about 28·5°N, and a subsidiary maximum at about 50°N. In the integration the subtropical maximum was initially quite weak, but by days 16-20 its speed

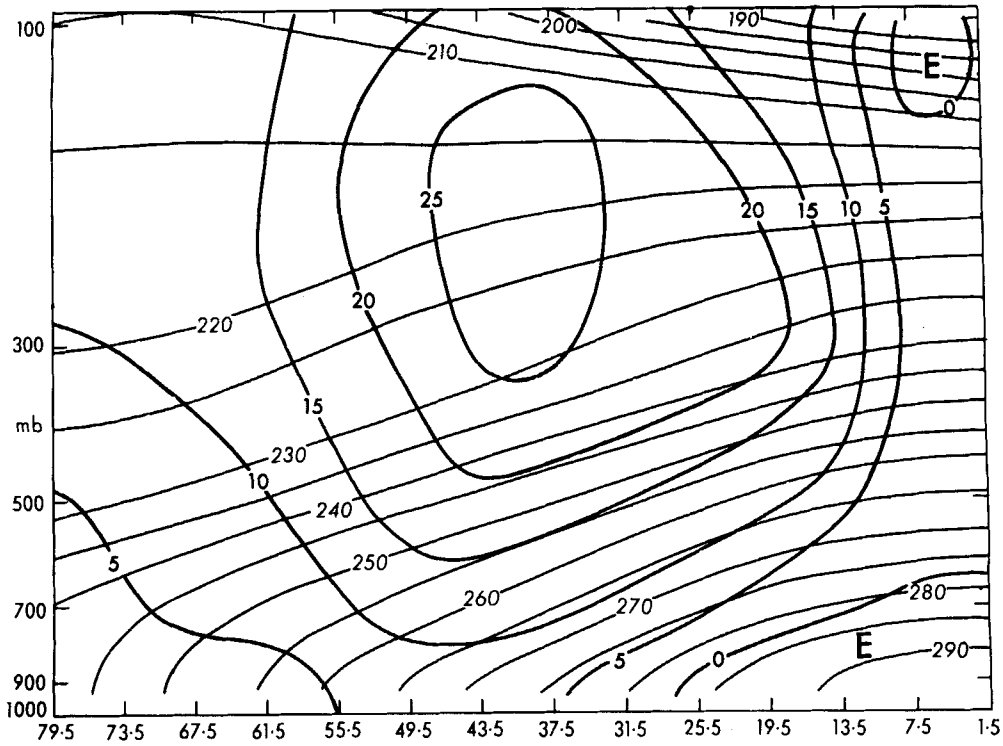

Figure 3(a). Caption opposite.

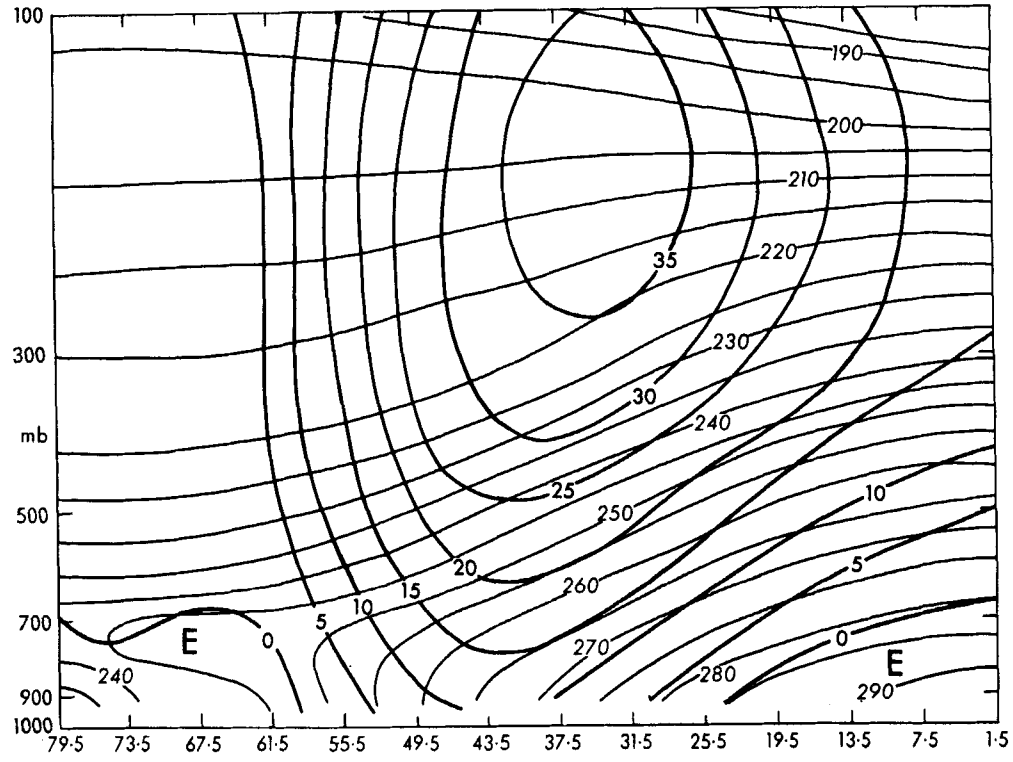

Figure 3(b). Caption opposite.

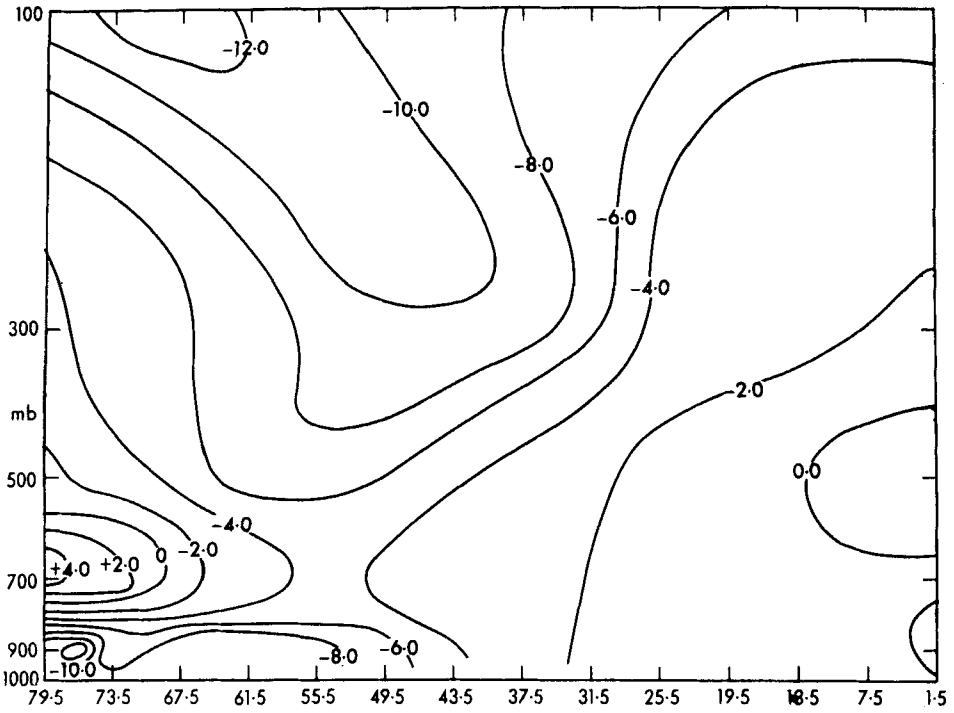

(c)

Figure 3. 5-day mean zonal cross-section of zonal wind and temperature. Units – m s^{-1} and °K.
(a) Days 1-5
(b) Days 56-60
(c) Temperature change from (a) to (b)

at 300 mb had increased to 40 m s^{-1} at 20°N. Throughout, there tended to be a double maximum, with a further minor maximum in high latitudes. These features are illustrated in Fig. 4(a) which is for the period 36-40 days.

(ii) 75°E (H & S Fig. 101). This longitude intersects the Himalayas, and the splitting of the jet-stream by them is a feature of the flow patterns (Staff members, Academia Sinica 1957). In the integration two westerly maxima were generally present, with continual change in their relative strengths. Their positions, however, were further south than in atmospheric cross-sections. Fig. 4(b) shows the cross-section for days 56-60, when both maxima were well developed.

(iii) 140°E (H & S Fig. 100). The mean atmospheric jet-stream here reaches speeds in excess of 70 m s^{-1} at 200 mb at about 34°N. Throughout the integration, a single maximum was maintained at about 32°N. During the first 50 days its speed increased only slightly, and then it decreased during the last 10 days (from 57 m s^{-1} to 49 m s^{-1} at 300 mb). However, in the final period, the strongest winds were at 100 mb, with maximum about 54 m s^{-1}. The main discrepancy between the atmospheric cross-sections and that for days 46-50 (Fig. 4(c)) is the weakness of the equatorial easterlies which for the atmosphere reach 10 m s^{-1} at 500 mb.

(iv) 180° (H & S Fig. 106). The atmospheric cross-section shows a rather weak single maximum of a little over 35 m s^{-1} at 200 mb at about 30°N. The model sections were very variable from one period to another with weak and ill-defined wind maxima. It is to be noted that in this region the model climatology did not accord closely with the January mean (see discussion in Section 5). The cross-section for days 46-50 (Fig. 4(d)) shows a comparatively well defined wind structure with a maximum at about 31°N, and a subsidiary maximum in very high latitudes.

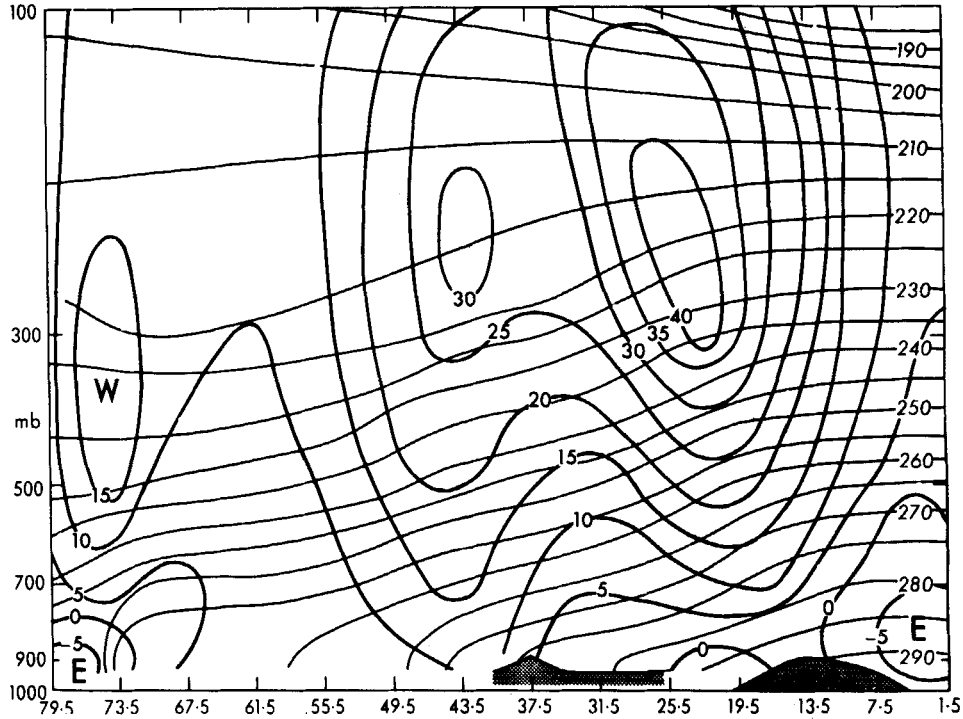

Figure 4(a). Caption on page 13.

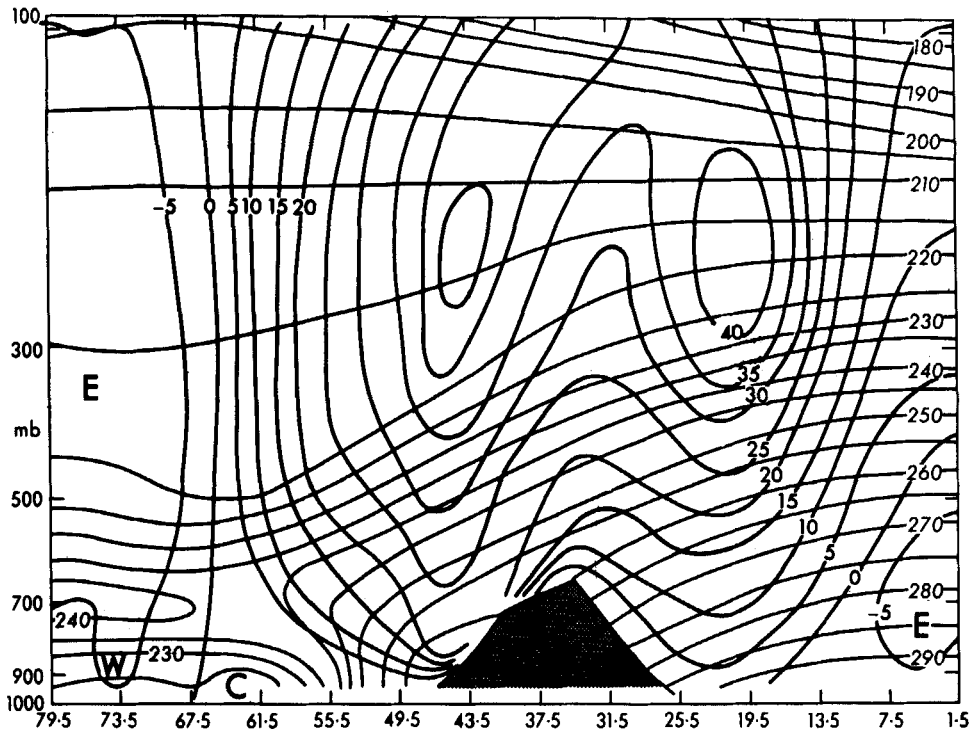

Figure 4(b). Caption on page 13.

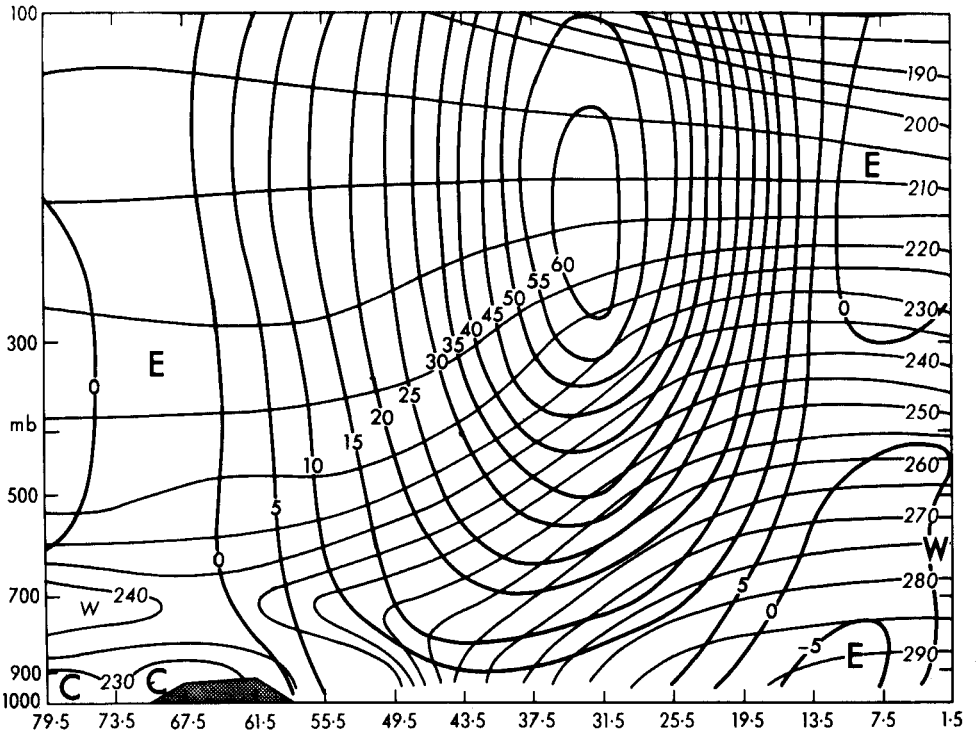

Figure 4(c). Caption on page 13.

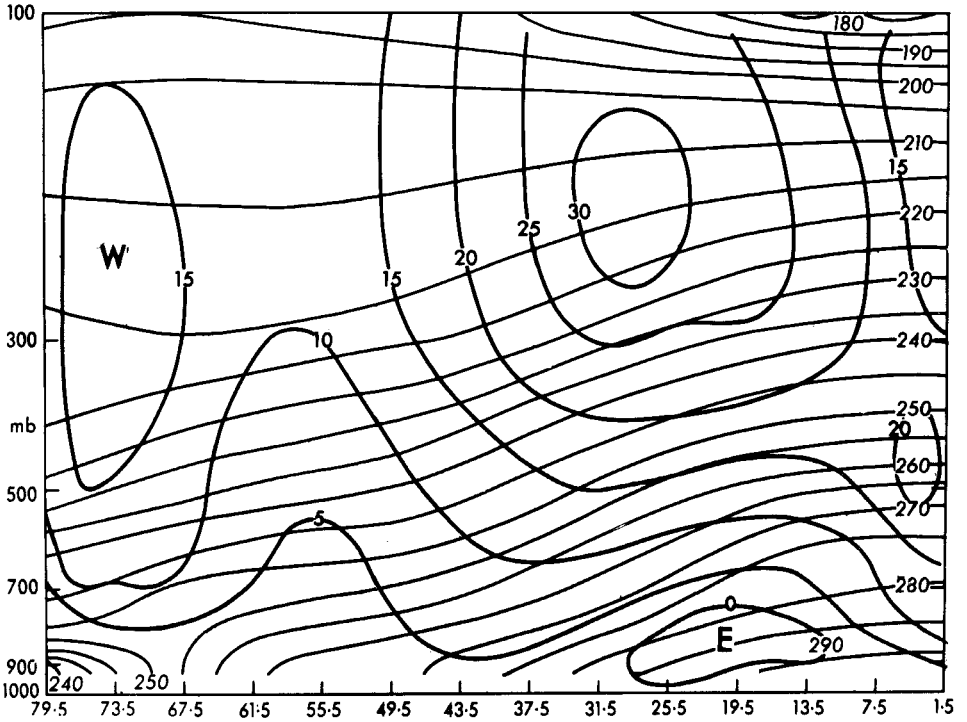

Figure 4(d). Caption on page 13.

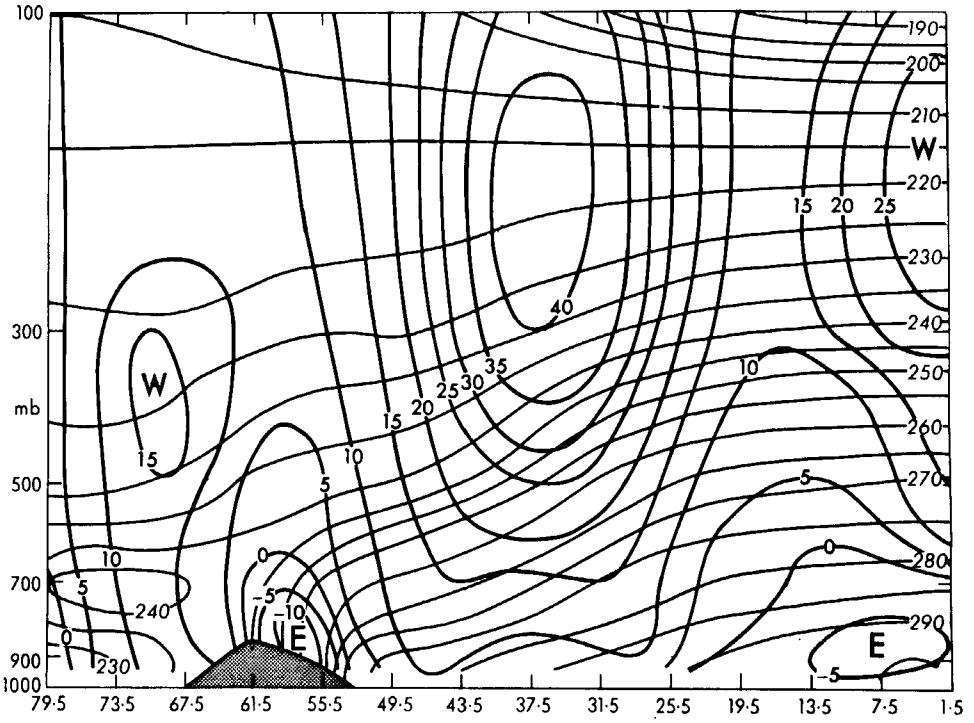

Figure 4(e). Caption on facing page.

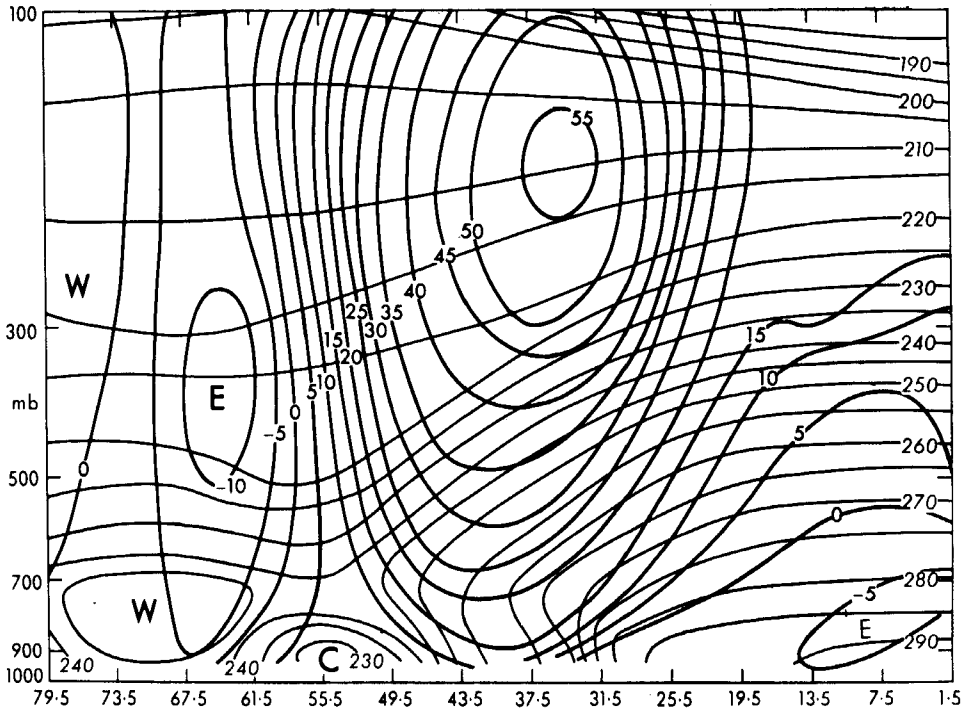

Figure 4(f). Caption on facing page.

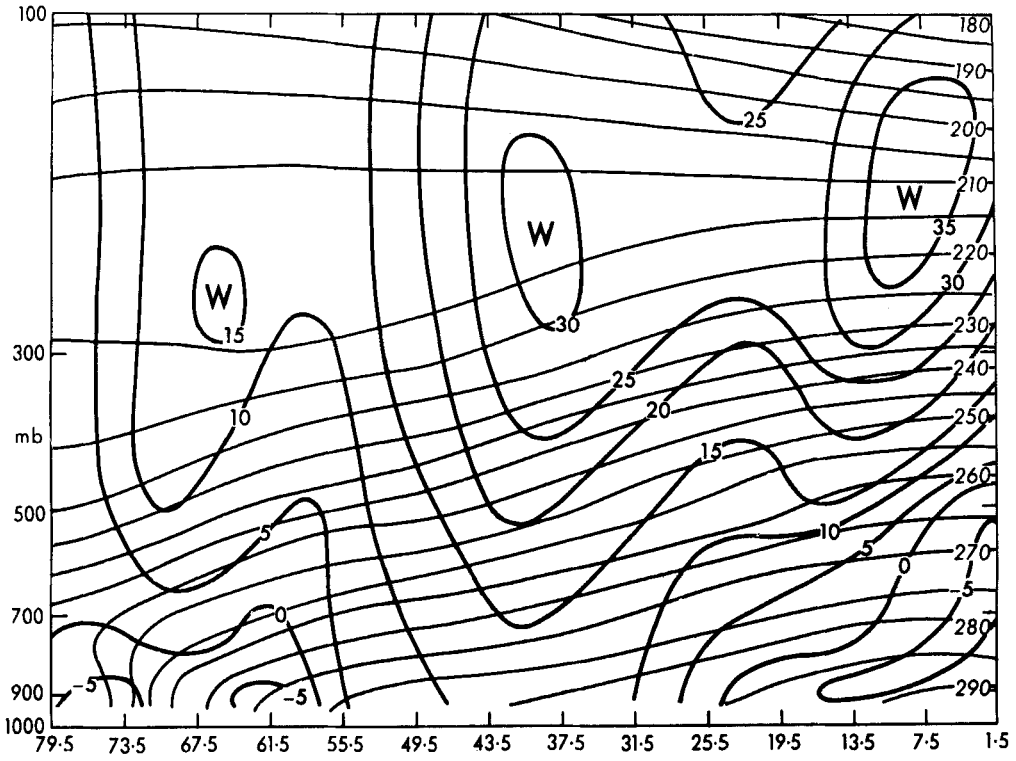

(g)

Figure 4. 5-day mean cross-section of zonal wind and temperature. Units m s^{-1} and °K.

(a) 40°E for days 36-40
(b) 75°E for days 56-60
(c) 140°E for days 46-50
(d) 180°W for days 46-50
(e) 130°W for days 36-40
(f) 80°W for days 56-60
(g) 10°W for days 56-60

(v) 130°W (H & S Fig. 105). The model cross-sections here tended again to be variable from one period to another, but throughout they were consistent in having fairly strong westerlies at upper levels near the Equator. The atmospheric cross-section also shows stronger equatorial westerlies than at any of the other longitudes illustrated. The middle latitude jet-stream tended to be rather far north in comparison with other longitudes, and fairly close to the atmospheric position (35-40°N). Thus the cross-section for days 36-40 (Fig. 4(e)) has a maximum of 40 m s^{-1} at 37·5°N at 300 mb.

(vi) 80°W (H & S 75°W Fig. 104). As at other longitudes, the model jet-stream is here farther south and stronger than in the atmosphere. Generally during the integration only a single maximum was found, but occasionally, a secondary maximum occurred near the Equator similar to that shown at 130°W. The strength of the winds tended to increase with time and the cross-section for days 56-60 (Fig. 4(f)) has higher wind speeds than any other period.

(vii) 10°W (H & S Fig. 103). At this line of longitude, the model usually had three wind maxima; one at low latitudes, which was continuous with the subtropical jet-stream found farther east at higher latitudes; a middle latitude jet-stream associated with the depression track across the Atlantic; and a weak maximum in high latitudes. The period days 56-60 is

typical (Fig. 4(g)). In the atmospheric cross-section, the first two maxima, though probably essentially the same in origin as those in the models are considerably farther north, while the third is absent.

4. The model's energetics

For the purpose of calculating energies and their transformations, the results obtained at sigma levels were interpolated on to the pressure levels 900, 700, 500, 300 and 100 mb. Interpolated values are given the suffix p. For temperature the interpolation assumed a constant lapse rate with height between the sigma levels, but for other variables the interpolation was simply linear in pressure. The averages on pressure levels were taken over points where values existed (because of topography some values were missing).

The following symbols are used:

$[\ ]$ denotes a zonal average, a function of pressure and latitude.

$\overline{[\ ]}^{H}$ denotes a hemispheric average, a function of pressure only.

The stability factor γ, which occurs in the expression for the available potential energy was evaluated for pressure levels 900, 700, 500, 300 and 100 mb from

$$\gamma = R/p(\overline{[\Delta T_p]}^{H}/\Delta p - K\overline{[T_p]}^{H}/p)$$

using a centred difference and $\Delta p = 400$ mb for the middle three levels, and a one-sided difference with $\Delta p = 200$ mb for the top and bottom levels of the atmosphere. The zonal available potential energy per unit mass was then taken as

$$\tfrac{1}{2}\gamma\, c_p\{[T_p] - \overline{[T_p]}^{H}\}^2$$

The variation of the hemispheric mean of the quantity with time for each of the 5 levels is shown in Fig 5(a). Fig. 5(b) contains similar graphs for the hemispheric mean values of the eddy available potential energy

$$\tfrac{1}{2}\gamma\, c_p\{T_p -]T_p[\}^2$$

The kinetic energy of the zonal mean flow was taken as

$$\tfrac{1}{2}\{[u_p]^2 + [v_p]^2\} \quad \text{per unit mass}$$

$[v_p]$ is of course small, and this quantity is little different from the kinetic energy of the mean zonal flow. To deal with the kinetic energy of the eddies, the kinetic energies of sigma layers at each point were first calculated and the values were attributed to the 200 mb pressure layers proportionately according to the overlap in pressure between the pressure and sigma layers. The small amounts of kinetic energy below 1,000 mb were neglected in this process. The eddy kinetic energy was then taken as the difference between the total kinetic energy and the kinetic energy of the zonal mean flow. The time variations of the hemispheric mean value of the zonal and eddy kinetic energies are shown in Fig. 5(c) and (d) respectively.

In comparison with the zonal mean kinetic energy as measured directly on the sigma surfaces, this method, because the mean surface pressure (p_*) is less than 1,000 mb, tends to increase values at the highest level (100 mb) at the expense of the lower levels. Table 1 contains values of zonal and eddy kinetic energies (for a more limited area) against which the variation with pressure level shown in Fig. 5(c) and (d) may be compared.

The transformations of zonal available and eddy available potential energy were calculated from

$$-R\{[T_p] - \overline{[T_p]}^{H}\}\{[w_p] - \overline{[w_p]}^{H}\}/p$$

and

$$-R\{T_p - [T_p]\}\{w_p - [w_p]\}/p$$

respectively. The graphs for the latter are in Fig. 5(e).

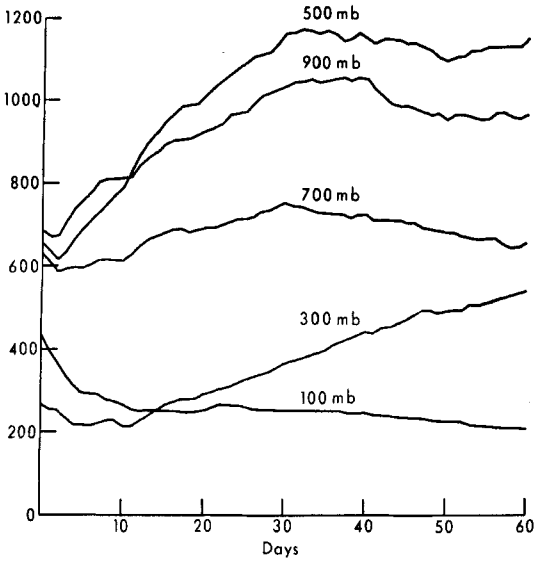

Figure 5(a). Caption on page 17.

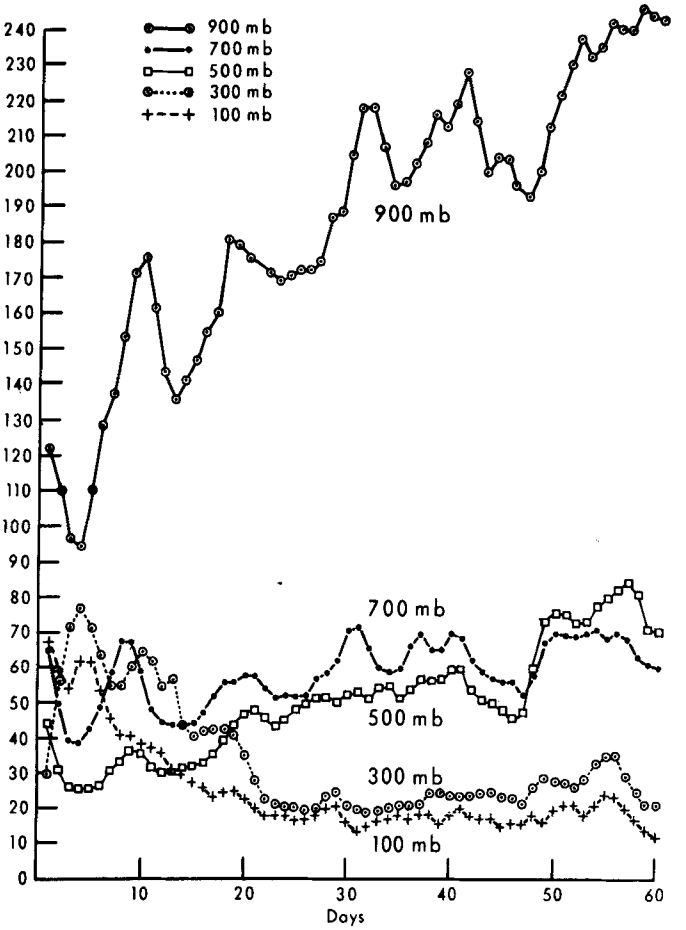

Figure 5(b). Caption on page 17.

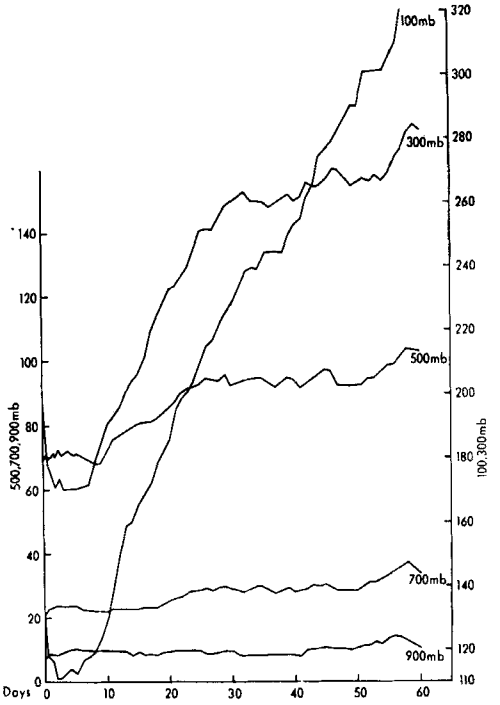

Figure 5(c). Caption on facing page.

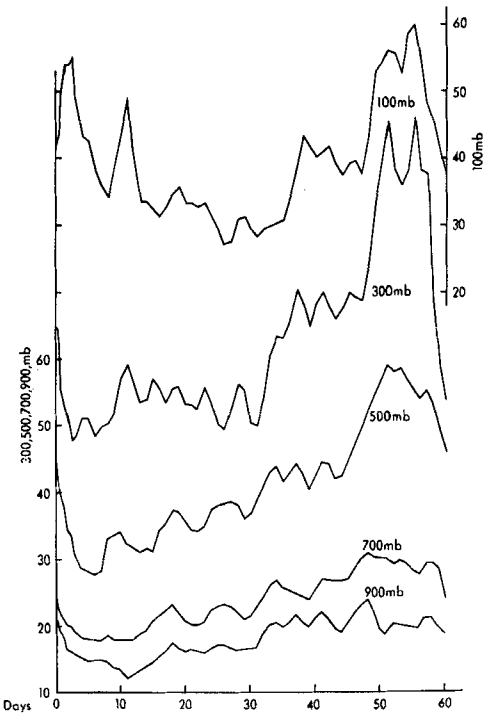

Figure 5(d). Caption on facing page.

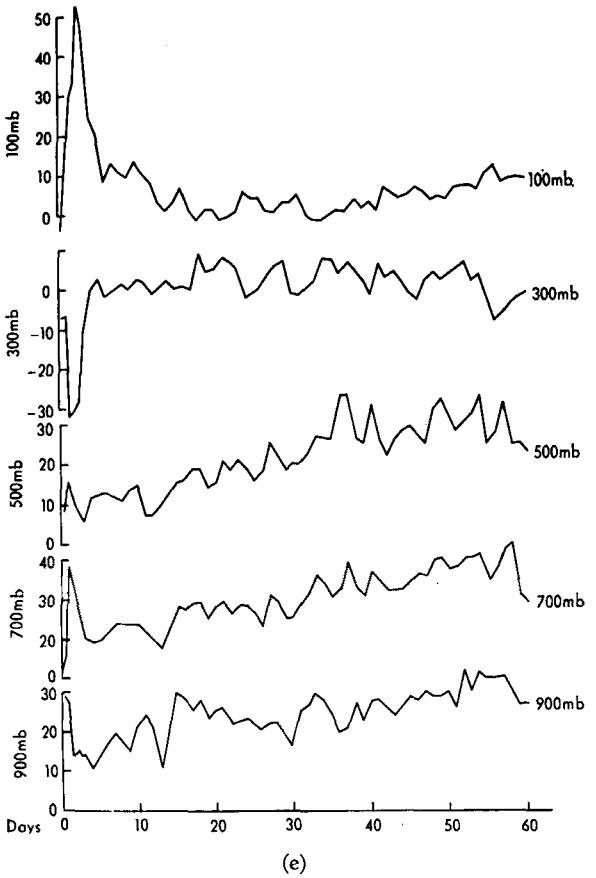

Figure 5. Hemispheric mean value of energy and energy tranformation for pressure levels most closely corresponding to the model's sigma levels plotted against time: Units: energies in 10^{-3} J gm^{-1}, transformations in 10^{-3} J gm^{-1} day^{-1}.

(a) Zonal available potential energy
(b) Eddy available potential energy
(c) Zonal kinetic energy
(d) Eddy kinetic energy
(e) Transformation of eddy available potential to kinetic energy

The zonal available potential energy (Fig. 5(a)) is greatest at 500 mb and 900 mb. The results of Wiin-Nielsen (1967) suggest that winter atmospheric values should be around 450, 600, 700, 250 and 100 in units of 10^{-3} J gm^{-1} in the slabs 1,000-800, 800 - 600, 600 - 400, 400 - 200 and 200 - 100 mb, respectively. These confirm the maximum in mid-troposphere but not the low-level maximum. Since the calculation on the initial data gave the largest value at 900 mb any discrepancy here is probably a consequence of the formulae employed; atmospheric cross-sections for winter, however, strongly suggest that a low-level maximum is realistic, and due essentially to the cooling of the atmosphere over middle and high latitude landmasses. The initial values of zonal available potential energy at middle levels are in accord with atmospheric estimations, but the 100 mb value is large, probably as a result of initialization procedures.

After a short-lived fall at the beginning of the integration which can be attributed to the effect of the vertical stabilization scheme in the Tropics, the zonal available potential energy rises steadily at tropospheric levels as a result of radiational cooling at middle and high latitudes. By day 30 or thereabouts the cooling at the lowest three levels is in balance with

diabatic heating and heat advection and thereafter the zonal available potential energy begins to decrease. At 300 mb, however, where the initial values are much smaller than at 500 and 700 mb, the zonal available energy continues to rise throughout the integration, and at the end has reached values comparable with those at the lower levels. The main factor contributing to this rise is net cooling in middle latitudes which is present even after 60 days. At 100 mb where there is a reversed temperature gradient between Pole and Equator, the available energy falls throughout the integration. The mean temperature at this level has also fallen substantially, and the decrease of available potential energy is caused by the greater rates of cooling in high than in low latitudes.

Like the zonal available potential energy, the eddy available potential energy (Fig. 5(b)) has a distinct maximum at 900 mb that is not indicated in atmospheric statistics (Wiin-Nielsen 1965; 1967). The values increase with time because the temperatures at the lowest level tend to follow the temperature at the Earth's surface, where the variance increases as the continents become progressively colder than the oceans whose temperatures are held fixed. The initial values at 700 and 500 mb appear small in comparison with Wiin-Nielsen's, ($\frac{1}{3}$ - $\frac{1}{4}$ the zonal available potential energy values) but this may be primarily due to the difference in areas involved in the calculation. At these two levels, an initial fall, probably reflecting a falling off in the energy of synoptic systems, is soon replaced by a gradual rise back to values similar to those at the beginning of the integration. Surprisingly, at 300 mb there is an initial rise, which Fig. 5(e) shows to be largely due to the conversion of kinetic to potential energy. It has been shown that at least some of this conversion takes place in developments near Japan, possibly as a down-stream effect of the Himalayas. The 100 mb graph falls from a large value to a small one, and then remains more or less constant. Like the zonal available potential energy at this level, the initial value is probably artificially high.

The mean zonal kinetic energy (Fig. 5(c)) shows on the whole the variation that would be expected from the temperature changes through the link with the thermal wind equation. The most notable feature is the continued steep increase at 100 mb, which would, if the integration were continued for a sufficiently long time lead to the transfer of the jet-stream maximum up to this level. In effect, in a longer integration the model would create an over-intense polar night jet-stream. No doubt this is in part accounted for by the solar radiation having been maintained at low winter values throughout the integration, for the atmosphere itself is dependent on the seasonal increase in radiation to reverse the cooling of the polar stratosphere. Overwhelmingly, however, the problems at this level are caused by vertical truncation. A more realistic simulation requires the presence of other levels above 100 mb, so that stratospheric meridional motions, and advection of heat from other levels can develop more freely.

The eddy kinetic energy (Fig. 5(d)) decreases rapidly in the first few days (except at 100 mb where there is an initial rise probably associated with the rise in eddy potential energy at 300 mb at the same time), and it continues at a fairly low level until around day 30, when there is a more or less rapid change to values typical of the initial conditions. Thereafter, the energy oscillates, with a period of a few days. At the upper levels there is a tendency for the oscillations to increase in amplitude, reflecting the tendency for baroclinic systems, whose origins are primarily at low levels, to extend progressively through greater depths. In particular, the 300 mb troughs associated with depressions during the last ten days of the experiment (when, as has just been seen, the zonal mean kinetic energy at this level was too great) were more intense, and more realistic than earlier.

Fig. 5(e) shows that at the lowest three levels, the transformation of eddy potential to kinetic energy had a rising trend from early in the integration with superimposed oscillations similar in period to those of the eddy kinetic energy. The largest values are at 700 mb. During the first few days the transformation at 300 mb is negative (i.e. kinetic to potential), and it then settles down to variations about some small value. This is probably unlike the real atmosphere and a consequence of vertical truncation (see, for example, Miyakoda, Smagorinsky, Strickler and Hembree (1969) who show the conversion obtained by using

ω's derived from an ω-equation and observed temperatures, and also from a model with more levels in the vertical than that considered here). In effect, the 300 mb level is intermediate between the lower three levels which are truly tropospheric and the top level which has a stratospheric temperature distribution; in consequence, although the mean meridional gradient tended to increase (Fig. 5(a)), the patterns associated with synoptic features remained weak and ill-defined (illustrated by Gilchrist 1971). For this level, the first few days of the experiment may be interpreted as a settling down period, in which it acquires the characteristics required by the model as a whole. Values at 100 mb are negatively correlated with those at 300 mb, due to the negative correlation of temperature between the two levels.

Fig. 6(a) and (b) illustrate the latitude/height distribution of eddy kinetic energy and

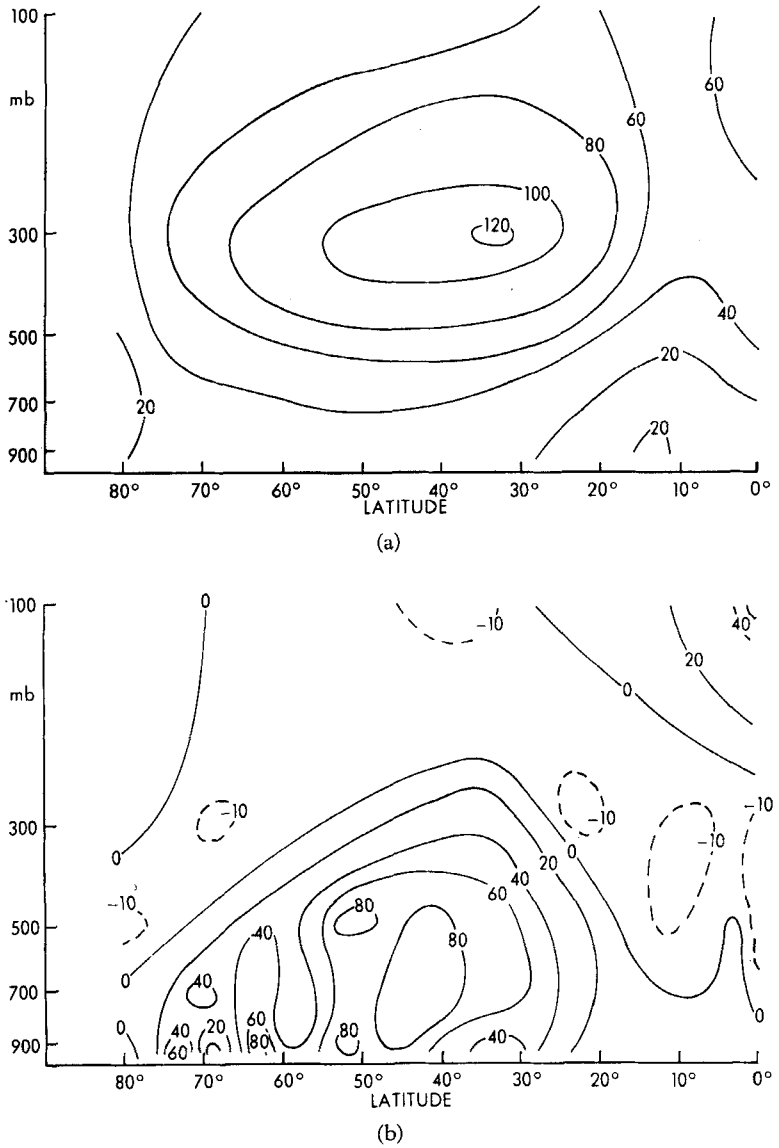

Figure 6. Latitude – pressure (height) distributions for days 51-60.

(a) Eddy kinetic energy. Units – 10^{-3} J gm^{-1}

(b) Transformation of eddy available potential to kinetic energy. Units – 10^{-3} J gm^{-1} day^{-1}.

the transformation of eddy potential to kinetic energy for the last 10 days of the experiment. In comparison with the atmospheric values of eddy kinetic energy for January (see Oort and Rasmusson, quoted by Manabe, Holloway and Stone (1970a)) the model values are much too small (~50 per cent) but they appear to be consistent with those obtained by other models using a similar grid-length. Qualitatively, however, the pattern follows that of the atmosphere fairly well except close to the Equator where the maximum should be at about 200 mb rather than at 100 mb as shown.

Apart from the local maxima at the lowest level, which are associated with variations of ω and T caused by topographic features, the region of large values of eddy potential to kinetic energy conversion (Fig. 6(b)) is in mid-troposphere at the latitudes where cyclonic development usually occurs in the model. The maximum is about $87{\cdot}5 \times 10^{-3}$ J gm^{-1} day^{-1} at 700 mb, 43·5°N. A region of predominantly negative values is found at 10-20°N, where, on the whole, air is descending in the downward limb of the tropical Hadley circulation. Above 500 mb, the values fall off rapidly, except close to the Equator, where a positive maximum is found at 100 mb, consistent with the maximum of eddy kinetic energy there. A region of positive conversion at 300 mb in equatorial latitudes was found by Manabe and Smagorinsky (1967) and Miyakoda *et al.* (1969) and its presence is apparently confirmed by the findings of Nitta (1970). It may be remarked that in this model, there is an association between upward motion and high temperatures at 300 mb near the Equator when the east Pacific values are omitted, but the overall correlation is destroyed by the inclusion of this area, where there is equatorial descent and comparatively high temperatures (see Section 5). Presumably, however, if there is a real difference between this model and those used in the above references, it stems mainly from the quite different methods of vertical stabilization. Another possibly significant difference is that here the representation of eddy viscosity in the thermodynamic equation does not depend explicitly on the flow.

From the energy integral calculations it is possible to construct the main parts of energy 'box-diagrams' showing the mean and eddy energies and their transformations. Fig. 7 shows the diagrams appropriate to the 10 day periods 21-30, 31-40, 41-50 and 51-60 days. The diagrams are not shown for earlier periods of the experiment since the presence of gravity waves falsifies the transformations unless more frequent sampling of the fields is carried out. The quantities that have been calculated directly are shown underlined; the other values have been inferred from the rates of change of the computed quantities, the rate of change assumed being between the mean values for the first and second five days of the 10 day period. Note that we have not calculated the transformation between zonal and eddy available potential energy, and therefore the 'source' term of these quantities contains it.

Among the quantities inferred from the rate of change of kinetic energy is the dissipation, for which there are two distinct mechanisms (i) by surface friction (F) i.e. implicit vertical mixing affecting only the lowest level of the model, and (ii) by the pseudo-viscosity term (D) which physically can be presumed to effect the flow of energy out of the system as a result of horizontal mixing with sub-grid-scale eddies. The relative magnitudes of the two types of dissipation are of considerable significance, and, therefore, they have been sampled at five day intervals to obtain a 'check' dissipation, taken as the average of the hemispheric mean values for days falling within a ten day period. As expected, the check total dissipation is approximately equal to the sum of the zonal and eddy dissipations derived by balance requirements from the energy rates of change. By assuming the check values, estimates have been made of the F and D values for the mean and eddy energies separately.

The estimates obtained in this way could be distorted by accumulated errors, but, on the whole, the values which emerge are reasonably consistent. The initial values of P_Z, P_E, K_Z and K_E were 513, 66, 85 and 40 in units of 10^{-3} J gm^{-1}, the first two rather higher than atmospheric estimations for reasons that have been considered. By days 51-60, P_Z and P_E have increased by about a third, being then higher than values obtained by

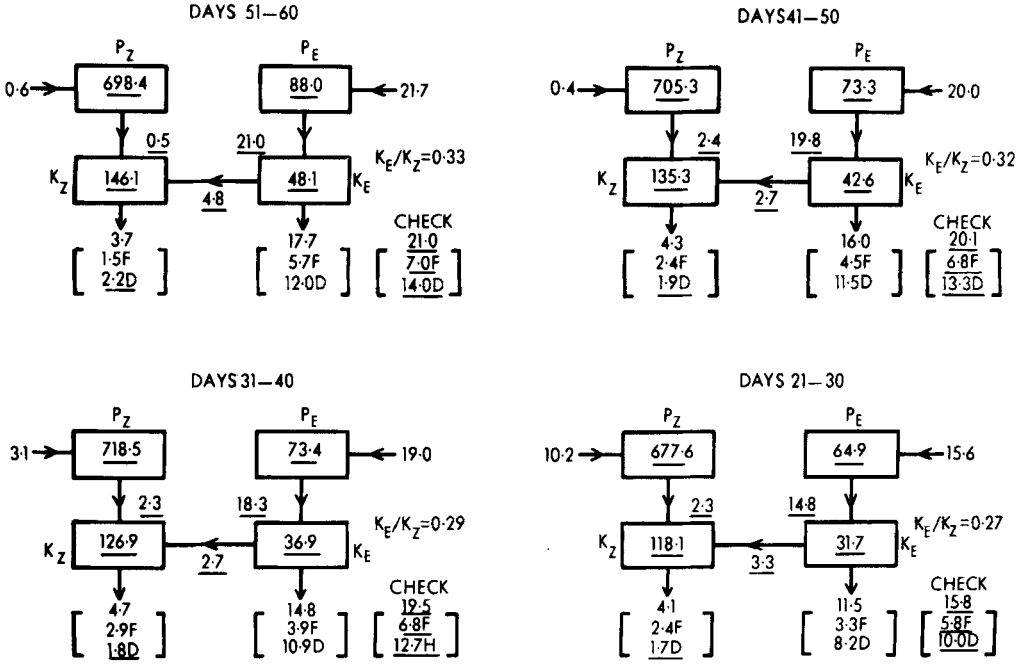

Figure 7. Mean hemispheric energy 'box-diagrams' for days 21-30, 31-40, 41-50, 51-60. P_Z, P_E – zonal and eddy available potential energy. K_Z, K_E – zonal and eddy kinetic energy. Units: energies in J cm^{-2}, transformations in J cm^{-2} day^{-1}. Quantities underlined have been calculated; others have been inferred from the rates of change of calculated quantities. F indicates dissipation by friction at the Earth's surface; D indicates dissipation by diffusion terms in the equations of motion. ' Check ' values refer to independent evaluations of the dissipation which should be approximately equal to values inferred from the energy changes.

Manabe, Smagorinsky, Holloway and Stone (1970b) with moist models, which, however, by virtue of using annual mean radiation amounts and omitting surface topographic variations, had a much smaller temperature variance in the lowest levels.

The zonal mean kinetic energy is much greater at the end of the experiment than at the beginning, though values for the troposphere alone are not so excessive. The ratio of eddy to zonal energy fell from 0·47 to 0·27 at days 21-30, but subsequently recovered to 0·33. Throughout the last 40 days of the integration, the dissipation by the pseudo-viscosity term was about twice that by surface friction. This is intermediate between the values of Manabe *et al.* (1970b) for an N40 (1·1) and an N20 (2·5) moist model; this model in these terms is approximately N30, i.e. 30 points between Equator and Pole.

The kinetic energy per unit mass on the sigma surfaces has been analysed spectrally for the area 15°N-75°N. Fig. 8 shows five day mean values in waves 1-18 through the integration, along with the initial values, and Table 1 presents, for each of the model levels separately, the energies in certain wavebands for particular periods.

Note that because of the difference in area, the energies in Table 1 are systematically higher than those shown in Fig. 5. Near the beginning of the experiment there were substantial energy reductions in waves 4-8, and of those only wave 5 subsequently reached energies as high as its initial value. This fall is indicative of a lack of baroclinic instability, particularly in the early stages of the experiment. Even in the last ten days, when the total eddy energy is similar to its initial value, there is a relative deficiency in this range (Table 1 (d)). For wave-numbers greater than 8, the energies during most of the integration were comparable with or slightly higher than the initial values. The largest changes are evident in waves 1-3. For the first half of the integration the total energy associated with them was comparable with that at the initial time, but, after this, at about the time when there was a

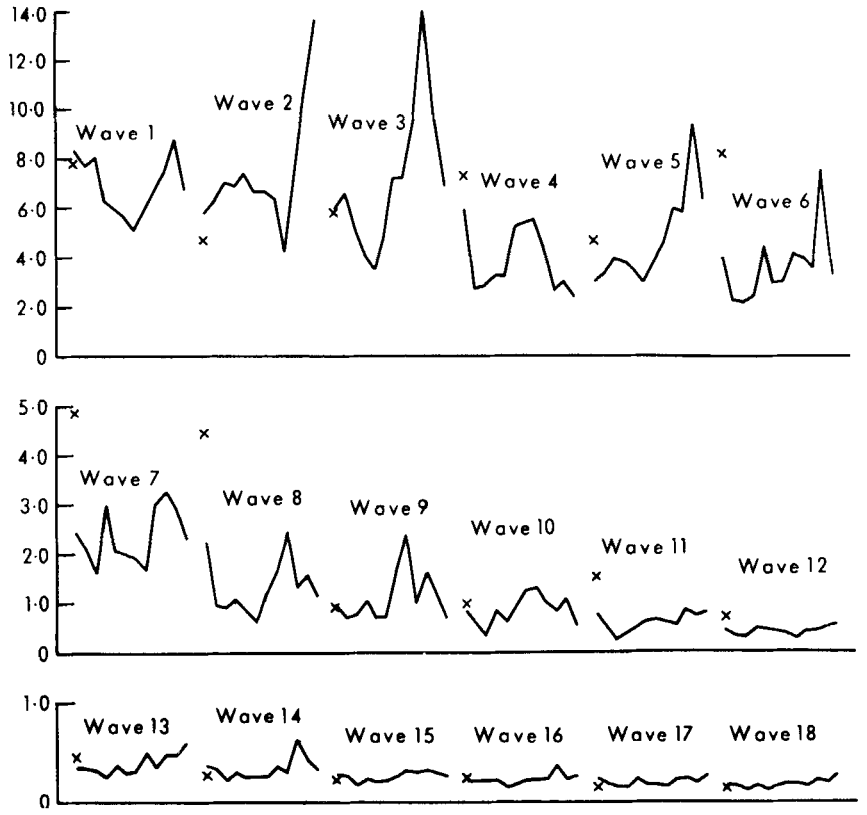

Figure 8. 5-day mean values of the energies in individual waves for the area 15°N-75°N plotted against time. X indicates the initial value of the kinetic energy in the wave-number. Units – J cm^{-2}.

notable increase in cyclonic activity, it increased markedly, firstly through the growth of wave-number 3, and later by the growth of wave-number 2. In the atmosphere waves 2 and 3 are usually quasi-stationary at positions fixed by the characteristics of the Earth's surface, and their intensity is maintained or intensified by baroclinic waves which develop preferentially on the eastern side of the major stationary troughs, this being the mechanism by which energy is passed from the baroclinic into the ultra-long waves. The course of events in the experiment suggests that the growth of waves 2 and 3 basically followed this pattern. In the period 40-50 days when wave 3 was dominant, the major troughs at about latitude 50°-60°N were over America (~110°W), over Europe (~10°E) and off the East Asian coast (~130°E). However, there was no marked ridging between the latter two and subsequently the dominance of wave two was established by their merging to form a broad trough over Asia at the same time as the trough over America moved to a more westerly position (see Fig. 10). These changes were accompanied by a reduction in surface pressure over central Asia (see Section 5(*a*)) and a slackening of the jet-stream at 140°E (see Section 2(*b*)). Manabe *et al.* (1970b) and Miyakoda, Strickler, Nappo, Baker and Hembree (1971) have remarked on the small amplitudes of the ultra-long waves in their models; and on the improvement obtained by increasing the grid resolution. In view of their findings, the behaviour of the ultra-long waves in this experiment is of particular interest; it indicates that even with a comparatively coarse mesh, the non-linear interactions between baroclinic and very long waves can be large when the long waves are already established climatological features of the model. It is to be noted that in Manabe *et al.* the model did not include the topographic features of the Earth's surface; and Miyakoda *et al.* were concerned with comparatively short integrations of up to 14 days.

TABLE 1. KINETIC ENERGY IN WAVEBANDS, FOR EACH LEVEL OF THE MODEL FOR AREA 15°N-75°N

(a) for the initial data;
and the average values for the periods
(b) 1-30 days (c) 31-60 days (d) 51-60 days.
Units – 10^{-3} J gm^{-1}

Wave-number range		0	1-3	4-8	9-13	14-18	1-18
$\sigma = 0{\cdot}1$	(a)	164·73	23·88	17·33	3·71	1·35	46·27
	(b)	209·95	24·32	14·13	1·67	0·64	40·76
	(c)	316·08	27·67	18·69	1·69	0·41	48·45
	(d)	343·56	35·31	21·52	1·39	0·66	58·88
$\sigma = 0{\cdot}3$	(a)	256·67	32·50	60·76	8·33	1·32	102·91
	(b)	267·43	32·09	27·32	4·21	1·75	65·37
	(c)	320·60	42·45	35·85	7·62	2·46	88·38
	(d)	330·63	53·06	40·00	7·11	2·38	102·55
$\sigma = 0{\cdot}5$	(a)	104·40	17·52	34·78	4·79	0·85	57·94
	(b)	116·17	19·11	13·15	2·76	1·04	36·06
	(c)	135·61	25·53	18·58	4·27	1·40	48·78
	(d)	141·09	35·43	21·23	3·75	1·49	51·90
$\sigma = 0{\cdot}7$	(a)	31·93	9·55	19·03	3·09	0·74	32·41
	(b)	38·41	10·71	6·71	1·77	0·75	19·40
	(c)	46·90	13·97	9·70	2·52	0·95	27·13
	(d)	54·03	13·70	11·02	2·20	0·96	27·87
$\sigma = 0{\cdot}9$	(a)	9·67	7·95	14·41	3·36	0·86	26·58
	(b)	12·59	7·94	6·97	2·89	0·96	18·76
	(c)	14·67	10·56	10·02	4·07	1·64	26·29
	(d)	17·96	9·74	11·31	3·64	1·62	26·30

TABLE 2. RATE OF DISSIPATION BY PSEUDO-VISCOSITY EXPRESSED AS THE FRACTIONAL DECREASE IN ENERGY PER DAY, FOR EACH LEVEL OF THE MODEL FOR PERIOD 31-60 DAYS FOR THE AREA 15°-75°N

Wave-Number	1	2	3	4	5	6	7	8	9
$\sigma = 0{\cdot}1$	0·07	0·05	0·06	0·10	0·07	0·10	0·14	0·19	0·22
$\sigma = 0{\cdot}3$	0·19	0·15	0·14	0·21	0·17	0·21	0·30	0·43	0·46
$\sigma = 0{\cdot}5$	0·14	0·11	0·13	0·18	0·15	0·19	0·27	0·38	0·42
$\sigma = 0{\cdot}7$	0·13	0·11	0·13	0·18	0·17	0·20	0·30	0·39	0·42
$\sigma = 0{\cdot}9$	0·20	0·29	0·29	0·36	0·38	0·40	0·47	0·70	0·68
All levels	0·15	0·12	0·14	0·20	0·16	0·19	0·29	0·42	0·45
	10	11	12	13	14	15	16	17	18
$\sigma = 0{\cdot}1$	0·29	0·36	0·43	0·46	0·51	0·75	0·68	0·70	0·75
$\sigma = 0{\cdot}3$	0·59	0·68	0·87	0·94	0·95	1·15	1·15	1·25	1·41
$\sigma = 0{\cdot}5$	0·48	0·58	0·73	0·77	0·80	0·97	0·97	1·07	1·12
$\sigma = 0{\cdot}7$	0·49	0·58	0·74	0·72	0·81	0·96	1·03	0·88	1·01
$\sigma = 0{\cdot}9$	0·84	0·97	1·10	1·21	1·18	1·46	1·41	1·58	1·55
All levels	0·58	0·69	0·85	0·90	0·93	1·14	1·13	1·23	1·30

The energy box-diagrams (Fig. 7) indicate that the rate of dissipation of eddy energy by the pseudo-viscosity term in the equations of motion amounts to about a quarter of the eddy energy total per day. In order to assess its dependence on wavelength, the dissipation has been evaluated for each wave-number 1-18 for each of the model levels. Table 2 shows the average dissipation for the period 31-60 days expressed as a fractional decrease in the energy per day. Thus for all levels taken together, about 1/7 of the energy of the longest waves is removed per day, while for wave-numbers greater than 14, the rate of depletion is such as to eliminate the energy in 1 day or less. This dependence on wave-number is less than might be expected from linearized approximations. There is significant dissipation not only of the very short waves, but of baroclinic and long waves as well. Similar conclusions were reached by Manabe *et al.* (1970b). It will also be noticed that the dissipation is relatively greatest at the lowest level and at the level of maximum zonal mean wind. The implication is that there is a strong non-linear effect, the damping of the long waves being relatively greater the greater the energy present in the short waves. This is in opposition to the desired non-linear effect of the dissipation term, and tends to reduce its effectiveness. Other formulations, including the simplest, i.e. a constant pseudo-viscosity coefficient, probably have the same behaviour, at least qualitatively, and the determination of the best formulation from this point of view requires further investigation.

5. The circulation at days 51-60

Features of the models' simulation have been further examined by considering the mean conditions in the period 51-60 days.

(*a*) *The mean sea-level pressure chart – Fig.* 9

The surface pressure is more zonal than a mean atmospheric chart for January. There is a polar anticyclone surrounded by a belt of low pressure mainly in latitudes 50°-60°N, a belt of subtropical high pressure mainly near 30°N and an equatorial trough. The most notable meridional feature is the trough in mid-Pacific, which breaks the sub-tropical anticyclone. The Asiatic high is much weaker and smaller than in the real atmosphere, and its position, over the eastern Himalayas rather than to the north of them suggests that the mechanisms maintaining it are not entirely realistic. The high on the initial chart (1,066 mb at 110°E, 55°N) moved south-eastwards and declined during the first few days of the experiment (as it also did to some extent in reality), and thereafter an intense Asiatic high was not established. Indeed, a depression track was established across the continent at about 60°N, with the depressions, on the whole, maintaining their intensity over land. Several factors may have contributed to this behaviour. The strong westerly flow, particularly marked over central Asia in the last ten days when wave number 2 had become dominant, may be the most important consideration. However, it seems possible that the surface friction formulation played a contributory rôle. It gives small or high values of the drag coefficient according as the lowest level is stable or unstable with respect to the underlying surface. Especially in the final stages of the integration when the Asian continent land temperatures were notably cold, this probably led to depressions experiencing a much higher drag over the sea than over land, and this reversal of the normally accepted pattern may have had an influence in establishing preferred cyclone tracks. There are, conceivably, other reasons, essentially more local in effect, which could have militated against the formation of a strong Asian anticyclone. Thus, the low level radiational cooling in high latitudes may be too small (see Section 5(*f*)) and it does not include effects due to the presence of cloud; the lack of definition in the lowest two kilometres of the model may also be of significance. Holloway and Manabe (1971) obtained a reasonable anticyclone with a high horizontal resolution, but a rather inadequate one with the resolution halved, indicating another possibly important consideration. However, the simulation of this feature by Mintz (1965) with a two-level low resolution model was very good, while Kasahara and

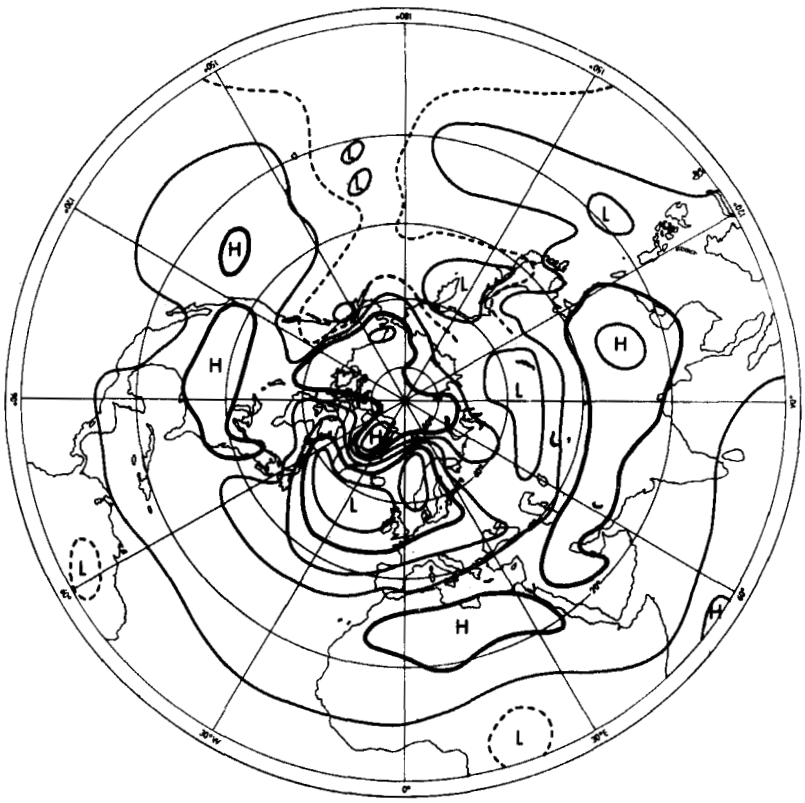

Figure 9. Mean sea-level pressure for days 51-60. Isobars at 8 mb intervals with 1,000 mb and 1,024 mb thickened. Dashed lines indicate additional intermediate isobars.

Washington (1971) using a six-layer model including dependence of the radiation on model cloud obtained a strong anticyclone, though their mean sea level pressure simulation was inadequate in certain other respects.

There is a notable difference between the pressure distribution in the Atlantic and Pacific, the reasons for which are not understood. The Icelandic low is deeper and further south than on the mean chart, and pressures over Europe are low, consistent with a persistent low latitude depression track, with depressions penetrating readily into the continent. In the Pacific, on the other hand, the low pressure area is split with two weak centres, one over Kamchatka, the other near the Aleutians. On the mean chart, the two oceans have similar pressure distributions, the Pacific low somewhat deeper than the Atlantic, and centred east of Kamchatka. The extent to which the Pacific distribution is due to the presence of a marked trough at low latitudes in mid-Pacific, or is merely consistent with it, requires further investigation (see Section 5(*c*)).

(*b*) *The* 500 mb *flow – Fig.* 10

The zonal flow is stronger than on the climatological mean chart, due principally to the intense centres over Canada and Siberia. At high latitudes, wave-number two is prominent, while at lower latitudes, a high proportion of the energy is in waves five and six. The trough in mid-Pacific which persisted through most of the integration is not present in the atmospheric mean. The other troughs are fairly well placed, but the ridges are generally weaker than observed. In equatorial regions, the surface low pressure areas (more or less coincident with the highest surface temperatures) are here overlain by relatively high contour values.

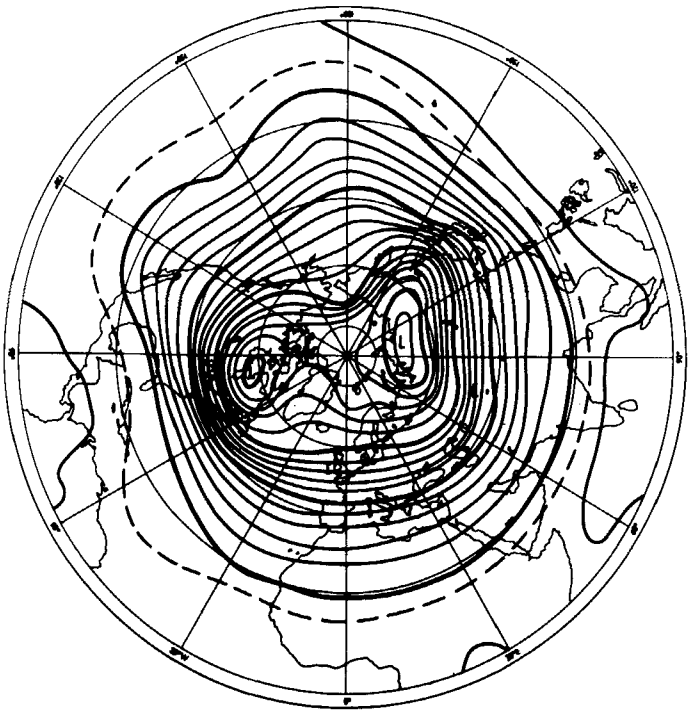

Figure 10. Mean 500 mb contour chart for days 51-60. Contours at 6 dm intervals, with 486, 516, 546 and 576 dm thickened. Dashed line is 579 dm.

Figure 11. Mean vertical motion (dp/dt) at $\sigma = 0{\cdot}5$ (approx 500 mb) for days 51-60. No shading – ascent less than 4 mb hr^{-1}, /// – ascent more than 4 mb hr^{-1}, dotted – descent less than 4 mb hr^{-1}, closely dotted – descent more than 4 mb hr^{-1}.

(*c*) *The vertical motion* (*dp*/*dt*) *at* sigma 0·5 (~500 mb) – *Fig.* 11

The strongest upward motion occurs close to the southern boundary, associated with the rising limb of the equatorial Hadley cell, and to the north there is a broader area of descent. This pattern, however, does not occur at all longitudes. Over virtually the whole of the eastern Pacific, subsidence extends to the Equator while ahead of the persistent trough in mid-Pacific, an area of strong ascent running north eastwards from the western Pacific interrupts the subtropical subsidence belt. A similar, though less well-developed pattern is evident over Africa. Rowntree (1972; and personal communication) has noted such patterns in another general circulation model, and has attributed them to the surface temperature distribution near the Equator; the sea surface temperature distribution in this experiment, colder in the eastern than in the western Pacific (see Fig. 1), corresponds to his 'cold' category.

In subtropical latitudes, there are areas of maximum descent just east of the Himalayas, in mid-Pacific and off the west coast of America, the wavelength being 60°-70° of longitude. Across the Atlantic and east of Japan the main depression tracks are marked by broad areas of small resultant ascent.

The rainfall follows this pattern of vertical motion rather closely. The equatorial rainfall is as high as 5·4 cm day^{-1} in the west Pacific, but other maxima at other longitudes are little more than half this amount. The areas of subtropical subsidence are virtually rainless, despite a relatively high humidity (75-90 per cent) at the lowest level of the model, caused by the assumption of moist conditions at the Earth's surface. In the same latitudes, the average daily rainfall rises to more than 2 cm ahead of the trough in mid-Pacific, and over the high ground in Mexico. The latter maximum is continuous with a belt of rain over the east Pacific at about 10-15°N, and may be a weak ITCZ formed away from the Equator, where, in these longitudes, there is subsidence. It is worth noting that this is consistent with the observed rainfall maximum which in the east Pacific is north of the Equator (Möller 1951). Along the track of the Atlantic depressions the rainfall maximum is 1·25 cm day^{-1} at 35·5°N, 55°W; the corresponding Pacific maximum east of Japan, however, is only a little more than half this amount.

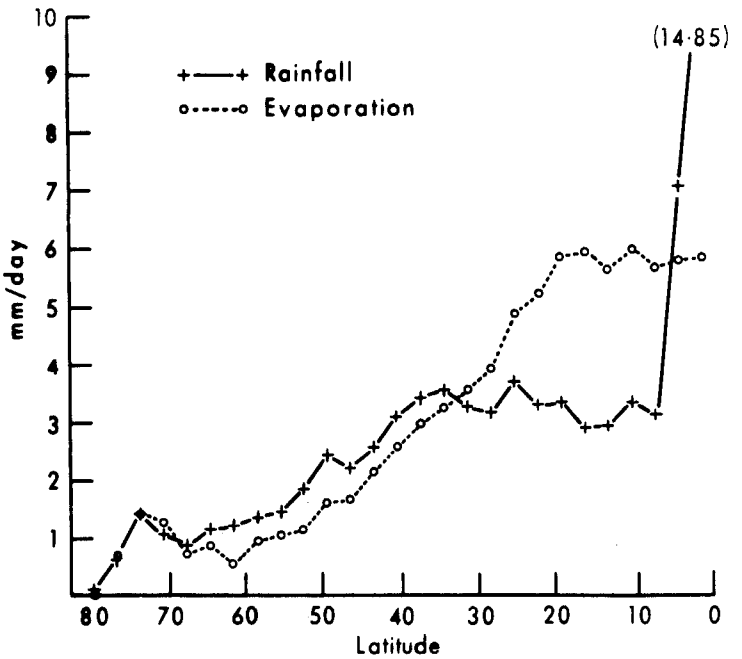

Figure 12. Zonal mean values of evaporation and rainfall for days 51-60. Units – mm day^{-1}.

(*d*) *The latitudinal distribution of rainfall and evaporation – Fig.* 12

During the experiment, when a humidity mixing ratio became negative (as a result of truncation error in the advective calculation), the value was replaced by zero. In examining the moisture balance of the model, it became clear that this procedure constituted a significant moisture source, especially in regions of persistent subsidence, since the truncation error is particularly large in vertical advection. The source had a maximum, both in absolute amount and as a proportion of the total evaporation, at 22·5°N, viz 0·8 mm day^{-1}; between 10°N and 30°N, it exceeded 0·5 mm day^{-1}, but outside this belt it fell off to small values. In constructing Fig. 12 this moisture source has been added to the calculated evaporation.

The region for which evaporation exceeds rainfall corresponds fairly well with observation (Newell, Vincent, Dopplick, Ferruzza and Kidson 1969), but at higher latitudes the excess of precipitation over evaporation remains rather small. The width of the equatorial rain belt is artificially narrow because of the boundary at the Equator. The highest values of evaporation clearly occur in cold dry air masses moving from a relatively cold continent over the sea. Apart from high values at isolated grid points in the Red Sea and Persian Gulf, amounts are greatest off the east coast of Asia, where there are values in excess of 10 mm day^{-1} in a strip of 2-3 grid points between latitudes 15° – 30°N. A similar region with slightly smaller values occurs at higher latitudes (30° – 45°N) off the American coast.

(*e*) *The mean meridional circulation – Fig.* 13

The meridional circulation may be compared with the January observed, given by Oort and Rasmusson (1970). The strength of the equatorial Hadley cell in the model is realistic. On the other hand, the low level flow is excessively concentrated while the return flow in the upper atmosphere is spread over much too deep a layer. This is at least partly due to vertical truncation and the absence of a computational level at the height of maximum flow (between 300 and 150 mb). The Ferrel cell of middle latitudes is too weak; the polar cell is fairly well represented.

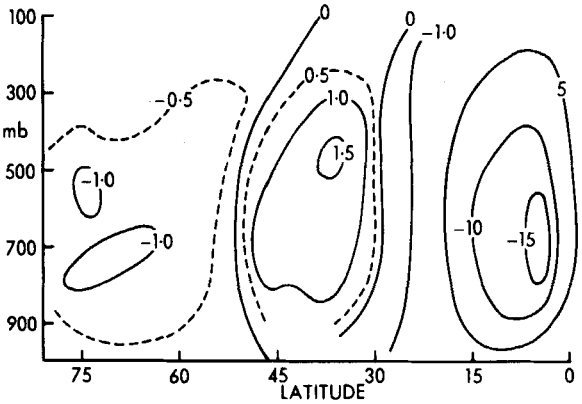

Figure 13. Mean meridional circulation for days 51-60. The iso-lines indicate the total mass transport northward below the level in units of 10^{13} gm s^{-1}.

(*f*) *The latitudinal distribution of diabatic heating – Fig.* 14

Fig. 14(a), (b), (c) and (d) show the heating due respectively to condensation in large-scale rainfall, to convective release of latent heat, to net radiation, and to exchange with the

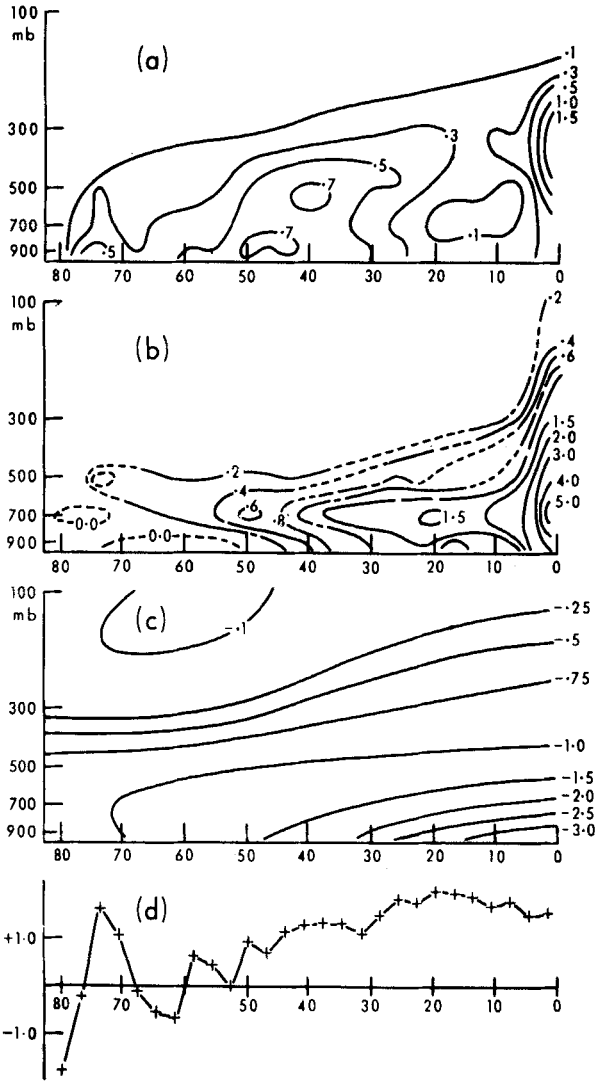

Figure 14. Mean zonal diabatic heating of the model atmosphere for days 51-60, Units – °K day^{-1}.
(a) Heating due to 'large-scale' rainfall i.e. rainfall resulting from explicit vertical motion.
(b) Heating due to 'convective' rainfall i.e. rainfall resulting from the application of vertical stabilization procedures.
(c) Net radiative cooling of the model atmosphere.
(d) Heating of the model's lowest level as a result of sensible heat exchange with the Earth's surface.

Earth's surface. The values have been obtained by sampling the data at daily intervals, and therefore they may not be entirely representative, particularly the convective heating which is very variable both in space and time; but the general pattern shown is unlikely to be significantly in error. These diabatic heating terms will tend to be balanced by the convergence of sensible heat plus potential energy (Fig. 15), though since we are dealing with a rather short period and also since the model cools throughout, a close balance cannot be expected. Diagrams of the mean atmospheric diabatic heating for December to February with which the model results can be compared, are shown by Newell *et al.* (1969).

The net radiational cooling is excessive at low-levels in low latitudes, though, from the results shown by Rodgers and Walshaw (1966), this does not appear to be essentially

due to the cooling to space approximation. Partly, it is caused by the neglect of cloud in dealing with infra-red radiation, but the possibility remains that a bias has arisen from the use of empirical emissivities. At higher latitudes, cooling at about 700 mb is notably less than the atmospheric values.

To a large extent, the excessive equatorial cooling is balanced by enhanced convective heating; the diabatic heating by latent heat release is much greater at low levels than estimated by Newell *et al.* Elsewhere, the values of latent heating, apart from a shift of the pattern southwards, are comparable with the atmospheric values. The maximum of sensible heating is also too far south, but at about 2°C per day is in good agreement with estimation for the real atmosphere.

(g) *The meridional flux of sensible heat plus potential energy – Fig.* 15

The values given by Oort (1971) have been plotted for comparison with the model's values. In the Tropics, the northward flux is much too small. In this region, the positive flux is due to the potential energy term, and it seems clear that the failure to reach the observed values is a result of the model's Hadley cell characteristics (see Fig. 13). If the upper flow were concentrated at around 200 mb then this feature would be much improved. The maximum in middle latitudes is also much less than observed. A major factor in this is probably the model's failure to produce large quasi-stationary meridional systems already noted in describing the surface pressure chart. A large proportion of the flux in Oort's data is derived from the standing eddy term. The relatively small heat flux is also consistent with the rather small values of long-wave cooling at high latitudes.

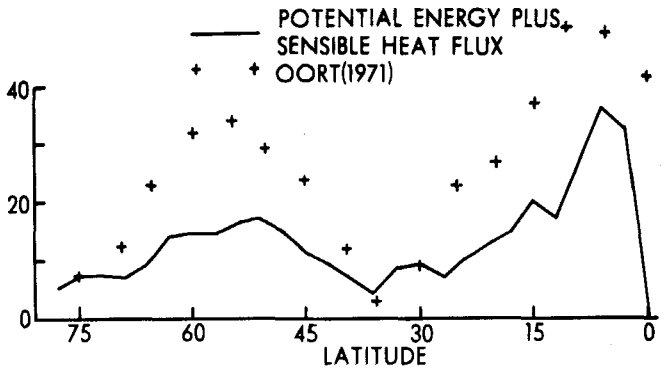

Figure 15. The meridional transport of sensible heat plus potential energy ($c_p T + \phi$) for days 51-60. Units – 10^{19} J day^{-1}.

(h) *The meridional flux of latent heat – Fig.* 16

Again, a comparison is made with Oort's data. Apart from a systematic shift to lower latitudes, the model values are in good agreement with the observed.

(i) *The latitudinal distribution of contributions to the change of angular momentum – Fig.* 17

The principal contributions to the change of angular momentum in latitude belts are (i) the flux convergence due to the motion, which is largely balanced by (ii) the surface torque and (iii) the mountain torque. Over a 10 day period, however, there is likely to be considerable departure from balance. The effect of horizontal diffusion on the angular momentum has not been considered; also it should be noted that the finite difference forms of the equations do not possess an exact conservation property for angular momentum.

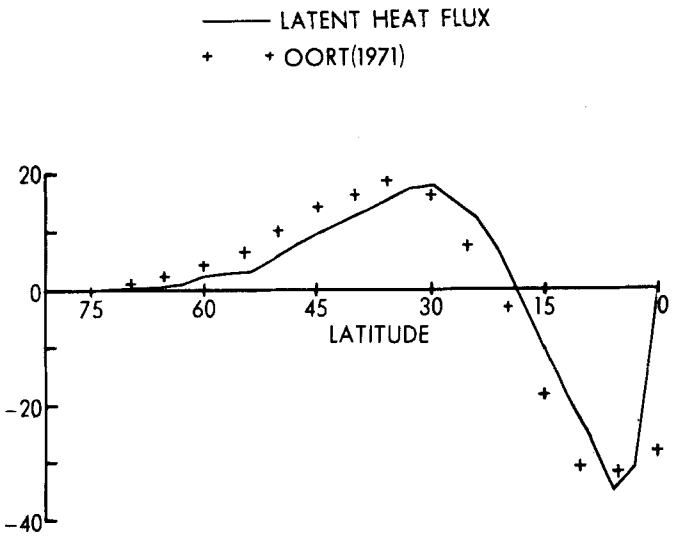

Figure 16. The meridional transport of latent heat for days 51-60. Units – 10^{19} J day^{-1}.

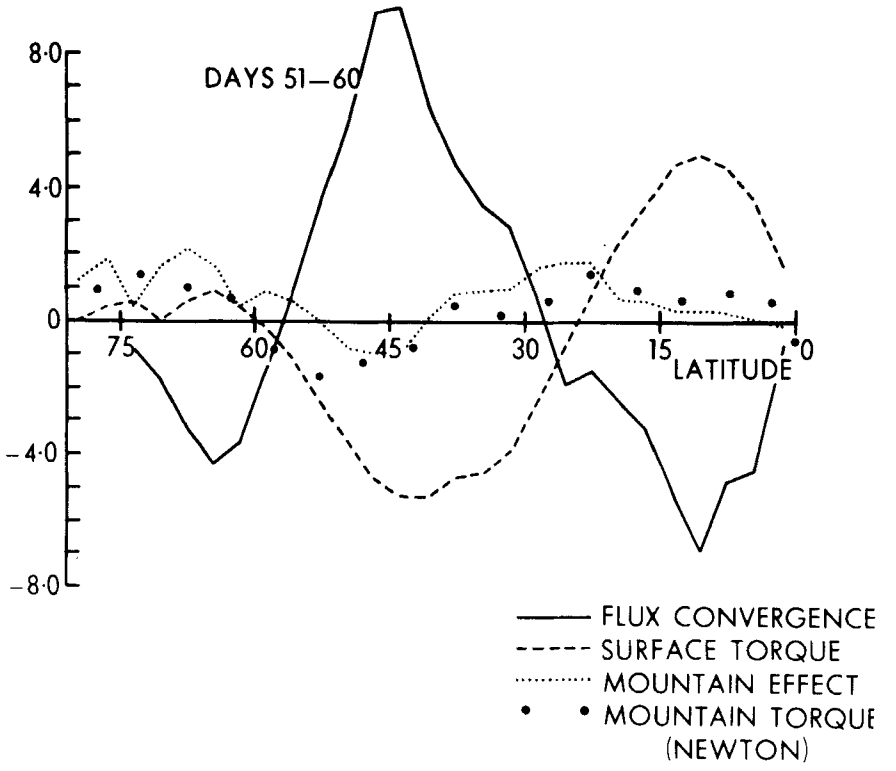

Figure 17. The mean rate of change of angular momentum for days 51-60 due to (i) the convergence of angular momentum (ii) surface torque and (iii) pressure differences across mountains. Units – 10^{8} dyne cm^{-1}.

The 'mountain effect' values have been obtained from an integration of the pressure gradient term in the zonal momentum equation through the atmosphere. For the analytical equations

$$\oint \int_0^1 \left(p_* \frac{\partial \phi}{\partial \lambda} + RT \frac{\partial p_*}{\partial \lambda} \right) d\sigma d\lambda = -\oint \phi_* \frac{\partial p_*}{\partial \lambda} d\lambda$$

and although this property does not hold exactly for the model equations, $\phi_* \delta_\lambda \overline{p_*}^\lambda$ and the vertically integrated pressure gradient term are generally of similar magnitude and sign. Recently Newton (1971) has given estimates of the mountain torque for January, and these have been added for comparison. Kasahara and Washington (1971) have published similar data for the NCAR model; it is interesting that their torque does not become positive in high latitudes.

The values for the model's surface torque agree fairly well with those estimated by Priestley (1951), though they tend to be shifted towards the Equator. Manabe *et al.* (1970b) and Kasahara and Washington (1971) show values of the surface torque for other models.

6. Conclusion

The major weakness in the formulation of the general circulation model which this experiment has revealed is a result of the number and disposition of levels in the vertical. A model level in the troposphere, experiencing net cooling by radiation, is able to reach an equilibrium temperature distribution because heat, sensible and latent, originating from the source at the Earth's surface, is transferred vertically by (primarily) implicit convective motions and horizontally by (primarily) explicit eddies. A level in the lower stratosphere, also experiencing net radiational cooling, is unable to tap the surface source of heat directly, and can only reach an equilibrium temperature distribution as a result of explicit vertical motions which transfer heat upwards from levels in the troposphere or downwards from levels which experience net heating through absorption by ozone. The model distribution of levels, which involves representing the top 200 mb by a single set of variables, among which the vertical motion in particular is constrained by the proximity (in finite difference terms) of the boundary on which the vertical velocity is zero, is not able to deal with this situation realistically.

Despite the deterioration in the upper part of the model, reasonable simulation was achieved of many tropospheric features. From about day 30 onwards, the synoptic simulations on a day-to-day basis were convincing, and led to mean features and variations at different longitudes that were typical of the atmosphere, even if, in some instances, they did not appear in the long term atmospheric average. Thus, a persistent trough in mid-Pacific, although not evident in the January climatological flow pattern, is often seen on mean charts. There were also, however, a number of things that were definitely incorrect. The failure to produce a strong Siberian high is probably the most disturbing of these; an examination of other model results, in which the adequacy of the simulation of this feature cannot easily be related either to the sophistication of the model or to particular facets of it, leave the reasons for this obscure as yet.

The experiment has also enabled us to map out the course by which the model, when presented with real atmospheric data, gradually approaches its own equilibrium state. It has seemed to us important to clarify this behaviour since there have been hopes that information of a statistical nature about future atmospheric developments might be forthcoming from general circulation models, using a fairly wide grid mesh, with atmospheric initial data and imposed, possibly time-varying, lower boundary conditions. Some of the characteristics displayed are perhaps peculiar to this model, but qualitatively at least we believe they apply to all. For the first ten days or so, the model lost eddy energy, and it was only by about day 30 that it was again approaching a state which could be considered fairly typical of the atmosphere. One would expect this period of regeneration to depend on the horizontal grid interval, and perhaps also on the number of levels in the vertical. Its reduction by improving these features is clearly very desirable. Other factors which might affect it require investigation – notably the effect of the pseudo-viscosity dissipation term. No formulation of a diffusion type that we are aware of is sufficiently discriminating with respect to scale to achieve a realistic dissipation at different parts of the spectrum with the grid length used in this experiment, and it is necessary to seek some compromise between excessive energy in the short waves and excessive damping of meteorological scales.

Alternatively, one might replace the term by a filter, which can be made highly scale-dependent (Shapiro 1971); preliminary results which we have obtained using this approach seem promising.

ACKNOWLEDGMENT

This paper is published with the permission of the Director General of the Meteorological Office.

REFERENCES

Corby, G. A., Gilchrist, A. and Newson, R. L. 1972 'A general circulation model of the atmosphere, suitable for long period integrations,' *Quart. J. R. Met. Soc.*, **98**, pp. 809-832.

Crutcher, H. L. 1971 'Selected meridional cross-sections of heights temperatures and dewpoints of the northern hemisphere,' NAVAIR-50-1C-59, Naval Weather Service Command, Washington.

Gilchrist, A. 1971 'An example of synoptic development in a general circulation model,' *Quart. J. R. Met. Soc.*, **97**, pp. 340-47.

Heastie, H. and Stephenson, P. M. 1960 'Upper winds over the world,' *Geophys. Memoirs* No. 103. HMSO, London.

Holloway, J. L. Jr. and Manabe, S. 1971 'Simulation of Climate by a Global General Circulation Model 1. Hydrologic cycle and heat balance,' *Mon. Weath. Rev.*, **99**, pp. 335-70.

Kasahara, A. and Washington, W. M. 1971 'General Circulation experiments with a six-layer NCAR model, including orography, cloudiness and surface temperature calculations,' *J. Atmos. Sci.*, **28**, pp. 657-701.

Longuet-Higgins, M. S. 1968 'The eigenfunctions of Laplace's tidal equations over a sphere,' *Phil. Trans. R. Soc. A.*, **262**, pp. 511-607.

Manabe, S., Holloway, J. L. Jr. and Stone, H. M. 1970a 'Tropical circulations in a time-integration of a global model of the atmosphere,' *J. Atmos. Sci.*, **27**, pp. 580-613.

Manabe, S. and Smagorinsky, J. 1967 'Simulated climatology of a general circulation model with a hydrologic cycle II: Analysis of the tropical atmosphere,' *Mon.Weath. Rev.*, **95**, pp. 155-169.

Manabe, S., Smagorinsky, J., Holloway, J. L. Jr. and Stone, H. M. 1970b 'Simulated climatology of a general circulation model with a hydrologic cycle III. Effects of increased horizontal computational resolution,' *Ibid.*, **98**, pp. 175-212.

Mintz, Y. 1965 'Very long-term integration of the primitive equations of atmospheric motion,' WMO *Technical Note* No. 66, pp. 141-167.

Miyakoda, K., Smagorinsky, J., Strickler, R. F. and Hembree, G. D. 1969 'Experimental extended predictions with a nine-level hemispheric model,' *Mon. Weath. Rev.*, **97**, pp. 1-76.

Miyakoda, K., Strickler, R. F., Nappo, C. J., Baker, P. L. and Hembree, G. D. 1971 'The effect of horizontal grid resolution in an atmospheric circulation model,' *J. Atmos. Sci.*, **28**, pp. 481-99.

Moller, F. 1951 'Vierteljahrskarten des Niederschlags fur die Ganze Erde,' *Petermanns Geographische Mitteilungen.*, **95**, pp. 1-7.

Newell, R. E., Vincent, D. G., Dopplick, T. G., Ferruzza, D. and Kidson, J. W. 1969 'The energy balance of the global atmosphere,' *The Global Circulation of the Atmosphere*. R. Met. Soc.

Newton, C. W. 1971 'Mountain torques in the global angular momentum balance,' *J. Atmos. Sci.*, **28**, pp. 623-28.

Nitta, T. 1970 'A study of generation and conversion of eddy available potential energy in the tropics,' *J. Met. Soc.*, Japan Ser.II **48**, pp. 524-28.

Oort, A. H. 1971 'The observed annual cycle in the meridional transport of atmospheric energy,' *J. Atmos. Sci.*, **28**, pp. 325-39.

Oort, A. H. and Rasmusson, E. M. 1970 'On the annual variation of the monthly mean meridional circulation,' *Mon.Weath. Rev.*, **98**, pp. 423-42.

Priestley, C. H. B. 1951 'A survey of the stress between the ocean and atmosphere,' *Australian J. Sci. Res., A* **4**, pp. 315-28.

Rodgers, C. D. and Walshaw, C. D. 1966 'The computation of infra-red cooling rate in planetary atmospheres,' *Quart. J. R. Met. Soc.*, **92**, pp. 67-92.

Rowntree, P. R. 1972 'The influence of the tropical east Pacific temperatures on the atmosphere,' *Ibid.*, **98**, pp. 290-321.

Shapiro, R. 1971 'The use of linear filtering as a parameterisation of atmospheric diffusion,' *J. Atmos. Sci.*, **28**, pp. 523-531.

Smagorinsky, J., Manabe, S. and Holloway, J. L. Jr. 1965 'Numerical results from a nine-level general circulation model of the atmosphere,' *Mon. Weath. Rev.*, **93**, pp. 727-768.

Staff Members, Academia Sinica 1957 'On the general circulation over Eastern Asia (1),' *Tellus*, **9**, pp. 432-446.

Wiin-Nielson, A. 1965 'Some new observational studies of energy and energy transformations in the atmosphere,' WMO *Technical Note* No. 66, pp. 177-202.

1967 'On the annual variation and spectral distribution of atmospheric energy,' *Tellus*, **19**, pp. 540-559.